

# Absorption enhancement of BC particles in a Mediterranean city and countryside: effect of PM chemistry, aging and trend analysis

Jesús Yus-Díez<sup>1,2</sup>, Marta Via<sup>1,2</sup>, Andrés Alastuey<sup>1</sup>, Angeliki Karanasiou<sup>1</sup>, María Cruz Minguillón<sup>1</sup>, Noemí Perez<sup>1</sup>, Xavier Querol<sup>1</sup>, Cristina Reche<sup>1</sup>, Matic Ivančič<sup>3</sup>, Martin Rigler<sup>3</sup>, and Marco Pandolfi<sup>1</sup>

<sup>1</sup>Institute of Environmental Assessment and Water Research (IDAEA-CSIC), Barcelona, 08034, Spain

<sup>2</sup>Grup de Meteorologia, Departament de Física Aplicada, Universitat de Barcelona, C/Martí i Franquès, 1, 08028, Barcelona, Spain

<sup>3</sup>Aerosol d.o.o., Ljubljana, Slovenia

**Correspondence:** Jesús Yus-Díez (jesus.yus@idaea.csic.es) and Marco Pandolfi (marco.pandolfi@idaea.csic.es)

## Abstract.

Black carbon (BC) is recognized as the most important warming agent among atmospheric aerosol particles. The absorption efficiency of pure BC is rather well known, nevertheless the mixing of BC with other aerosol particles can enhance the BC light absorption efficiency, thus directly affecting the Earth radiative balance. The effects on climate of the BC absorption enhancement due to the mixing with these aerosols is not yet well constrained because these effects depend on the availability of material for mixing with BC, thus creating regional variations.

Here we present the mass absorption cross-section, MAC, and absorption enhancement of BC particles, ( $E_{abs}$ ), at different wavelengths (from 370 nm to 880 nm for on-line measurements and at 637 nm for off-line measurements) measured at two sites in the Western Mediterranean, namely Barcelona (BCN; urban background) and Montseny (MSY; regional background).   
  $E_{abs}$  values ranged between 1.24 and 1.51 at the urban station depending on the season and wavelength used as well as on the pure BC MAC used as a reference. The largest contribution to  $E_{abs}$  was due to the internal mixing of BC particles with other aerosol compounds, on average between a 91 and a 100 % at 370 and 880 nm, respectively. Additionally, 14.5 and 4.6% of the total enhancement at the short-UV (370 nm) was due to externally mixed BrC particles during the cold and the warm period, respectively. On average, at MSY station, a higher  $E_{abs}$  value was observed (1.83 at 637 nm) compared to BCN (1.37 at 637 nm), which was associated to the higher fraction of organic aerosols available for BC coating at the regional station, as denoted by the higher OC:EC ratio observed at MSY compared to BCN. At both BCN and MSY  $E_{abs}$  showed an exponential increase with the amount of non-refractory (NR) material available for coating ( $R_{NR-PM}$ ). The  $E_{abs}$  at 637 nm at MSY regional station reached values up to 3 during episodes with high  $R_{NR-PM}$ , whereas in BCN  $E_{abs}$  kept values lower than 2 due to the lower relative amount of coating materials measured at BCN compared to MSY. The main sources of organic aerosols influencing  $E_{abs}$  throughout the year were HOA and COA (primary OA from traffic and cooking emissions, respectively) at both 370 nm and 880 nm. At the short-UV wavelength (370 nm), a strong contribution to  $E_{abs}$  from BBOA (biomass burning OA) and LO-OOA (less-oxygenated OA) sources was observed in the colder period. Moreover, we found an increase of  $E_{abs}$  with the aging state of the particles, especially during the colder period. This increase of  $E_{abs}$  with particle aging was associated to a larger relative amount of secondary organic aerosols (SOA) compared to primary OA (POA). The availability of a long dataset at both

25 stations from off-line measurements enabled a decade-long trend analysis of  $E_{abs}$  at 637 nm, that showed positive statistically significant trends of  $E_{abs}$  during the warmer months at MSY station. This s.s. positive trend at MSY mirrored the observed increase of the OC:EC ratio with time. Moreover, in BCN during the COVID-19 lockdown in spring 2020 we observed a sharp increase of  $E_{abs}$  due to the observed sharp increase of OC to elemental carbon (EC) ratio. Our results show similar values of  $E_{abs}$  to those found in the literature for similar background stations.

## 30 1 Introduction

The light-absorbing properties of atmospheric carbonaceous aerosols, i.e. black carbon (BC) and organic aerosols (OA), have been linked with a strong positive radiative forcing effect on Earth's energy budget (Liu et al., 2015; Zhang et al., 2018; Cappa et al., 2019). Recent scientific assessments(e.g. IPCC, 2021) on the global warming effect of anthropogenic agents have estimated that BC is the major aerosol contributing to the absorption of solar radiation from the ultraviolet to the infrared 35 part of the spectrum, with a direct radiative forcing (DRF) of  $0.71 \pm 0.17 \text{ W m}^{-2}$  (Bond et al., 2013). However, the DRF of carbonaceous aerosols still presents large uncertainties given the limitations to constrain the spatial distribution, mixing state, and absorbing properties of these atmospheric aerosols in climate models (e.g. IPCC, 2021).

BC particles can be mixed with less-absorbing and non-absorbing material through either external mixing, an heterogeneous mixture of internally homogeneous particles, or internal mixing, either an homogeneous mixture of internally homogeneous particles or an heterogeneous mixture of particle composition and population (Bond and Bergstrom, 2006). The mixing state of BC with these aerosol particles determines its mass absorption cross-section (MAC), which is a spectral quantity relating the volumetric absorptive efficiency of a particle per unit mass, and is usually reported in square meters per gram [ $\text{m}^2 \text{ g}^{-1}$ ]. The MAC of pure BC (or elemental carbon, EC, depending on the measuring technique employed Lack et al., 2014) is rather well constrained. However, BC aggregates are rarely emitted as pure BC as they are usually co-emitted and internally mixed with 40 other source-dependent aerosols that can enhance the MAC of BC (e.g. Bond and Bergstrom, 2006; Knox et al., 2009; Lack and Cappa, 2010). Moreover, the absorption of radiation by less-absorbing particles externally mixed with BC, as absorbing OA also referred to as brown carbon (BrC) (Andreae and Gelencsér, 2006), also contributes to increase the measured absorption 45 (Lack and Cappa, 2010). Different mixing states of BC particles were the cause for the regional differences found for the MAC in different background sites in Europe (Zanatta et al., 2016). The enhancement that this mixing produces in the resulting 50 observed MAC with respect to the theoretical pure BC MAC is defined as the absorption enhancement ( $E_{abs}$ ). Understanding the relationship of  $E_{abs}$  with the BC mixing state and the different aerosol species/sources is key to better parametrise the BC impact on radiative forcing (Jacobson, 2001; Bond et al., 2013). Whilst several studies assume  $E_{abs}$  as only influenced by the internal mixing (e.g., Lack and Cappa, 2010), we used here an approach similar to Liu et al. (2015) where the spectral enhancement of light absorption by BC is considered as due to both the external and internal mixing of BC particles.

55 Externally mixed BrC particles also contribute to the enhancement of total absorption, although the absorption efficiency of BrC significantly decreases from UV moving into the visible (e.g. Moise et al., 2015; Laskin et al., 2015; Samset et al., 2018; Saleh et al., 2018; Saleh, 2020). BrC absorption coefficient values found in the literature display a large spatial variability (e.g.

Liu et al., 2015; Saleh et al., 2018; Saleh, 2020; Zhang et al., 2020) due to the specific organic aerosol sources and composition found for each site. These differences in OA composition result in different BrC MACs, since different OA from different sources present absorption efficiencies variations (e.g. Saleh et al., 2018; Saleh, 2020; Zhang et al., 2020). Moreover, the MAC of different OA compounds shows different behaviour along the UV-visible range, hence the variation found in the influence of BrC on the absorption for this spectral range (Saleh et al., 2018; Saleh, 2020). The internal mixing contribution to  $E_{abs}$  has been thoroughly studied both through core-shell models (Lack and Cappa, 2010) and by laboratory and field experiments (e.g. Cappa et al., 2019). The main differences in  $E_{abs}$  values reported in literature were associated to different diameter of both BC cores and shell in the case of model simulations, and to BC aging in the case of laboratory and field experiments. In fact, BC particles aging can be seen as a surrogate of the particles shell diameter since more ageing implies more coating layers (Lack and Cappa, 2010). Therefore, analyzing the influence on  $E_{abs}$  of both internal and external BC mixing states is fundamental for a correct characterization of the aerosol particles light absorption and to better constrain modelling results (Liu et al., 2015).

Several laboratory studies, field measurements and modeling results can be found in the literature about  $E_{abs}$  values (e.g., Lack and Cappa, 2010; Cappa et al., 2012; Liu et al., 2015; Zhang et al., 2018). However, the results fail to present an ubiquitous  $E_{abs}$  value, with values ranging between almost no absorption enhancement ( $E_{abs} \sim 1$ , Cappa et al., 2012), to around a 50% absorption increase as assumed by some climate models ( $E_{abs} \sim 1.5$ , Liu et al., 2015, , and references therein), up to values of more than a 100%, especially at the shorter wavelengths where the BrC externally mixed can largely contribute to the  $E_{abs}$  (e.g. Chen et al., 2017). As a consequence of the broad spectrum of values, several authors have suggested to treat  $E_{abs}$  as a regional specific parameter in climate models to account for the different sources or processes that may contribute to increase both the amount of BrC and the degree of BC internal mixing (Lack et al., 2012; Liu et al., 2015; Zhang et al., 2018).

To characterize the specific chemical species or sources that affect and to which extent the  $E_{abs}$ , simultaneous measurements of aerosol particle light-absorption at multiple wavelengths, elemental carbon (EC) concentrations, and particulate matter chemical composition analysis are needed. Although specific instrumentation (e.g. the single particle photometer, SP2; and the soot particle aerosol mass spectrometer, SP-AMS) can be used for direct measurements of the chemical composition and internal mixing state of carbonaceous particles, their global implementation is sparse, thus impinging a global characterization of  $E_{abs}$  values. Using more simple yet robust monitors to obtain the source-dependent chemical composition influencing the absorption enhancement is possible (e.g. Zhang et al., 2018). The applied methodology consists on obtaining each measurement, e.g. chemical speciation, EC concentrations, light absorption, and aerosol aging through independent instruments, and merging the results to the lowest timestamp possible.

Here we present an analysis of the BC light absorption enhancement measured at an urban station (Barcelona; BCN) and a regional station (Montseny; MSY) in the Western Mediterranean basin. The chemical analyses were performed using offline 24-hour filter measurements at both stations (between 2010 and 2020). In BCN online chemical composition measurements with a higher time resolution were also available (2018). In BCN, EC measurements were performed with a semi-continuous SUNSET analyzer (Karanasiou et al., 2020) and submicron aerosol particles chemical composition measurements were performed with an Aerosol Chemical Speciation Monitor (ACSM; Via et al., 2021). Absorption measurements were performed with multiple-wavelength Aethalometer (AE33) and multi-angle absorption photometer (MAAP) instruments. In Sect. 3.1 we present an

overall analysis of both MAC and  $E_{abs}$ , showing the  $E_{abs}$  seasonal variability and the contribution of both external and internal BC mixing states to  $E_{abs}$ . In Sect. 3.2, we performed an analysis of the relationship between the absorption enhancement and 95 the amount of non-refractory material available for coating with BC particles. Sect. 3.3 reports the results of a multi-linear regression analysis performed to identify the main sources/species responsible for the increase of  $E_{abs}$  at both sites. Sect. 3.4 presents the influence of particle aging in the  $E_{abs}$  values. Finally, we performed a trend analysis of  $E_{abs}$  using the decade-long offline filter measurements available at both stations (Sect. 3.5). To the best of our knowledge, although some studies have 100 shown the variability of MAC in the Mediterranean basin (e.g. Pandolfi et al., 2014b; Zanatta et al., 2016), this is the first study of  $E_{abs}$  in this region and one of the few studies of its kind performed in Europe (Liu et al., 2015; Zhang et al., 2018).

## 2 Methodology

### 2.1 Aerosol sampling sites and main characteristics

Measurements were performed at Barcelona – Palau Reial (BCN, urban background, Barcelona,  $41^{\circ}23'24.01''N, 02^{\circ}6'58.06''E$ , 80 m a.s.l.), and Montseny (MSY, regional background, El Brull,  $41^{\circ}46'46''N, 02^{\circ}21'29''E$ , 720 m a.s.l.) monitoring supersites (NE Spain). These measurement stations are characterized by aerosols with different physical and chemical properties. BCN urban station is located within the Barcelona metropolitan area of nearly 4.5 million inhabitants at a distance of about 5 km from the coast, and at 200 m distance from one of the most concurred roads of the city ( $> 60k$  vehicles per day; City council of Barcelona). MSY regional station is located in a hilly and densely forested area within the Natural Park and Biosphere Reserve of Montseny, 50 km to the N–NE of the Barcelona and 25 km from the Mediterranean coast. A detailed characterization of these measurement stations can be found in previous works (e.g. Querol et al. (2001); Rodríguez et al. (2001); 105 Reche et al. (2011); Brines et al. (2014, 2015); Ealo et al. (2018) for BCN; and Pérez et al. (2008); Pey et al. (2009); Pandolfi et al. (2011, 2014a, 2016) for MSY. These supersites are part of the Catalonian Air Quality Monitoring Network and are 110 part of ACTRIS and GAW networks. Aerosol optical properties at BCN and MSY are measured following standard protocols (WMO/GAW, 2016).

115 Overall, the area of study is characterized by high concentrations of both primary and secondary aerosols from diverse emission sources (Rodríguez et al., 2002; Pandolfi et al., 2014a; Dayan et al., 2017; Rivas et al., 2020; Brean et al., 2020). Recently, Veld et al. (2021) presented the main aerosol sources in BCN and MSY by applying receptor modelling techniques to offline 24-hour speciated  $PM_{2.5}$  samples collected during the period 2009–2018. The main sources identified from OA 120 were the secondary OA (SOA), and from the secondary inorganic aerosols (SIA) they were sulphates, nitrates and ammonia. Moreover, online ACSM measurements at BCN station (Via et al., 2021) have also shown that the organic aerosols are mainly 125 dominated by secondary aerosols, also referred as oxygenated OA (OOA), as well as by hydrocarbon and cooking related OA (HOA and COA). Both Via et al. (2021) and Veld et al. (2021) have shown an increasing trend in the SOA as well as a reduction in the primary OA (POA) relative contribution to PM at BCN and MSY stations, mainly related with more restrictive pollutant emission policies and a larger amount of higher oxidative potential scenarios. The higher oxidative potential of the OA is characterized by an increase in the relative proportion of the more-oxidized, MO-OOA, in comparison with the less-oxidized

OOA, LO-OOA (Via et al., 2021). Finally, a common characteristic of BCN and MSY measurement sites is that both are located in the proximity of North African deserts, thus both sites are heavily impacted by Sahara dust outbreaks (Querol et al., 2009; Yus-Díez et al., 2020). For this reason, in order to avoid the interference due to dust absorption, we filtered out scenarios when the sites were under the influence of dust outbreaks (following the European Commission guidelines; European Commission, 130 2011).

## 2.2 Absorption coefficients and EC measurements

At both measurement sites, aerosol particle absorption coefficients ( $b_{abs}$ ) at 637 nm were obtained with multi angle absorption photometers (MAAP, Model 5012, Thermo Inc., USA, Petzold and Schönlinner, 2004). Moreover, in BCN absorption measurements were also performed with a multi-wavelength aethalometer (model AE33, Magee Scientific, Aerosol d.o.o. Drinovec 135 et al., 2015) at seven different wavelengths (370, 470, 520, 590, 660, 880 and 950 nm). The MAAP absorption coefficients at 637 nm were derived by the internal MAAP software using a radiative transfer model from the measurements of transmission of light through the filter tape and backscattering of light at two different angles, and corrections were made following Müller et al. (2011). MAAP measurements were obtained with a 1 min time resolution at a flow rate of 5 l/min and with a  $PM_{10}$  inlet 140 cut-off. The AE33  $b_{abs}$  coefficients in BCN were derived with the same time resolution and flow rate as the MAAP and with  $PM_{2.5}$  inlet. The aethalometer filter loading effect was corrected online by the dual-spot manufacturer correction (Drinovec et al., 2015), and the multiple scattering correction parameter, C, was set to 2.44, as obtained for the BCN station by Yus-Díez et al. (2021). Absorption measurements errors of 12% and 23% were set for the MAAP and AE33, respectively (Petzold and Schönlinner, 2004; Rigler et al., 2020). For the AE33, the larger uncertainty is introduced by the multiple scattering parameter, C ( $\delta C = \pm 0.57$  at BCN Yus-Díez et al., 2021), which depends on the physical properties of the particles collected on the filter 145 tape. In Yus-Díez et al. (2021) the C was found to have an average value of 2.44, and it did not present a marked dependence with the single scattering albedo (SSA) of the particles collected on the filter-tape. In fact, Yus-Díez et al. (2021) showed that the C values can considerably increase when SSA is high ( $> 0.95$ ). However, these high SSA are rarely measured in the city of Barcelona. Moreover, it was reported that the C is wavelength independent in Barcelona (cf. Fig. 1 Yus-Díez et al., 2021). Therefore, we used here the average C value of 2.44 for the deriving the absorption measurements.

150  $PM_{10}$  24-hour offline filter samples were collected at both BCN and MSY on 150 mm quartz micro-fibre filters (Pallflex 2500 QAT-UP) using high-volume samplers (MCV CAV-A and DIGITEL DH80 at  $30 \text{ m}^3 \text{ h}^{-1}$ ). The 24-hour average concentrations of major and trace element, and soluble ions (determined following the procedure by Querol et al. (2001)), as well as those of organic (OC) and elemental (EC) carbon (by a thermal-optical carbon analyser, SUNSET, following the EUSAAR2 protocol (Cavalli et al., 2010)) were obtained from these offline filter samples and were estimated to have a measurement error of 10%.

155 Semi-continuous EC measurements were obtained in BCN by means of a Semi-Continuous OC:EC aerosol analyzer (Sunset Laboratory Inc.) with a  $PM_{2.5}$  inlet cut-off at a flow rate of 8.0 l/min, a measuring interval of 3 hours using the EUSAAR2 protocol, with a measurement error of 10% (Karanasiou et al., 2020). The device was equipped with a C parallel-plate diffusion denuder to remove VOCs that can be adsorbed on quartz fibre filters and cause positive artefacts in the OC measurement (Viana et al., 2006). By comparing the EC measurements from the online and offline OC:EC measurements (Fig. S1) we show that

160 there is a good agreement between both techniques, and that on average offline EC concentrations in the PM10 fraction were 26% higher compared with online EC concentrations in the PM2.5 fraction during the 2018 period measurement. .

### 2.3 Submicron non-refractory PM chemical composition measurements and OA source apportionment

165 A Quadrupole Aerosol Chemical Speciation Monitor (Q-ACSM, Aerodyne Research Inc.) was deployed in BCN for chemical speciation of submicrometric particles at a flow rate of 3 l/min. The incoming particles go through an aerodynamical lens transmitting particles of aerodynamic diameters from 75 to 650nm. Then, these particles are vaporized, ionized by hard-electron impact and fragmentated and the resulting fragments are analyzed by a quadrupole mass spectrometer. The instrument can provide using a fragmentation table (Allan et al., 2004) the concentrations of non-refractory PM<sub>1</sub> species (OA, sulphate, nitrate, ammonia and chloride) with 30 min resolution and a 12-120 Th OA spectra matrix. The software used for data acquisition and treatment was provided by Aerodyne Inc. (versions 1.6.0.0 and 1.6.1.1, respectively) and implemented in the Igor Pro 170 (Wavemetrics, Inc.) environment).

175 The OA matrices retrieved were used as input for Positive Matrix Factorization analysis (PMF; Paatero and Tapper, 1994), applied using multi-linear engine (ME-2) (Paatero, 1999) to differentiate the different OA sources. A detailed description of the OA sources detected in BCN and used in this work can be found in Via et al. (2021). Briefly, the OA sources in BCN were: Cooking-like OA (COA), Hydrocarbon-like OA (HOA), Biomass Burning OA (BBOA), Less-Oxidized Oxygenated OA (LO-OOA) and More Oxidized Oxygenated OA (MO-OOA).

### 2.4 Determination of the absorption enhancement, E<sub>abs</sub>

Here, similarly to Zhang et al. (2018), we derived E<sub>abs</sub> as the ratio between the measured ambient mass absorption cross-section (MAC) calculated at the different wavelengths available from the AE33 and the MAAP, and the reference MAC value of pure BC.

180 The observed ambient MAC defines the contribution to the measured absorption coefficients from BC particles internally and externally mixed with organic and inorganic species that can contribute positively to the measured absorption (Bond et al., 2013). The ambient MAC measurements were obtained as the ratio of the light absorption coefficients (b<sub>abs</sub>) at a given wavelength,  $\lambda$ , and the elemental carbon (EC) concentrations obtained with the Sunset analyzer, either online or offline,

$$\text{MAC}^\lambda = \frac{b_{\text{abs}}^\lambda}{[\text{EC}]} \quad (1)$$

185 The enhancement of the absorption due to both internal and external mixing of the BC particles can be quantified by normalizing the measured ambient MAC <sup>$\lambda$</sup>  with a reference value for pure BC, MAC <sup>$\lambda$</sup> <sub>ref</sub>. As already stated, we have applied here the same methodology to determine E<sub>abs</sub> as in Zhang et al. (2018) and Liu et al. (2015) by calculating the ambient MAC through equation (1) applied to the 7 AE33 wavelengths. Thus, since BrC absorbs more efficiently at the shortest wavelengths (370-470 nm mostly) but not at 880 nm, the observed E<sub>abs</sub> at the shortest wavelengths includes the lensing-driven enhancement

190 and the enhancement induced by semi-volatile BrC (e.g. Liu et al., 2015), whereas the observed  $E_{abs}$  at 880 nm represents the lensing-driven enhancement only.

$$E_{abs}^{\lambda} = \frac{MAC^{\lambda}}{MAC_{ref}^{\lambda}}. \quad (2)$$

195 The reference MAC,  $MAC_{ref}^{\lambda}$ , can be obtained either from the literature (Bond and Bergstrom, 2006), or from the experimental data. There are two experimental approaches for obtaining  $MAC_{ref}^{\lambda}$ : 1) by using denuded measurements that evaporate the semi-volatile organic and inorganic species thus allowing for a measurement of the pure BC absorption (e.g. Liu et al., 2015), and 2) by using as  $MAC_{ref}^{\lambda}$  the intercept of the relationship between the ambient  $MAC^{\lambda}$  and the OC:EC ratio. In this letter case  $MAC_{ref}^{\lambda}$  is the MAC value obtained when the OC:EC ratio is equal to 0 (Zhang et al., 2018). Here we have preferentially used the second method (intercept) to determine the reference value for  $MAC_{ref}^{\lambda}$  (Fig. S2-S4). For this purpose we used a Deming regression fit taking into account the propagation of errors from the absorption and OC:EC measurement errors.

200 Additionally, we also used the literature MAC reference value to calculate  $E_{abs}$ , i.e.  $7.5 \pm 1.2 (m^2 g^{-1})$  at 550 nm (Bond and Bergstrom, 2006), which was extrapolated to each AE33 wavelength assuming an Absorption Ångström Exponent (AAE) of 1.

205 Online  $MAC^{\lambda}$  and  $E_{abs}^{\lambda}$  values at BCN were obtained using AE33  $b_{abs}^{\lambda}$  coefficients averaged to the semi-continuous Sunset OC:EC measurements time stamp (3h) during 2018 when the Q-ACSM measurements were also available. Offline MAC values at both BCN and MSY were obtained by using 24-hour average  $b_{abs}$  coefficients from the MAAP at 637 nm, and 24h OC:EC concentrations from  $PM_{10}$  filters (2010-2020). Figure S6 shows the obtained  $MAC_{ref}^{\lambda}$  values for both BCN and MSY stations for all the wavelengths available from both online (BCN) and offline (BCN and MSY) measurements. Data in Fig. S6 were grouped into two periods: a cold period from December to May, and a warm period from June to October. As shown later, measurements were grouped into these two distinct periods due to the source apportionment results from Q-ACSM 210 measurements in BCN, since the BBOA-like compounds were only detected during winter and spring (Via et al., 2021). Offline  $MAC_{ref}^{\lambda}$  values at both stations showed a good agreement with the reference theoretical value obtained in Bond and Bergstrom (2006), whereas the online measurements obtained with the AE33 were higher through-out the whole spectrum. Similar higher than the theoretical  $MAC_{ref}^{\lambda}$  values have also been reported in other studies, such as in Zhang et al. (2018).

215 Furthermore, we have assumed here that BrC particles do not absorb at 880 nm (Kirchstetter et al., 2004) and that the measured absorption at this wavelength was only driven by the BC internally mixed particles (i.e. the lensing effect). Moreover, although some studies assumed a wavelength independent lensing-driven absorption enhancement for BC particles (Liu et al., 2015; Zhang et al., 2018), other studies showed that the presence of brown coatings can produce variations in the spectral behaviour of  $E_{abs}$  with the wavelength (Lack and Cappa, 2010). Consequently, in order to take into account the possible influences of the brown coatings on  $E_{abs}$ , following Lack and Langridge (2013) we performed a sensitivity study by studying 220 the variation of the absorption enhancement attributed to BC, the BC coating and BrC by varying the absorption Ångström

exponent (AAE) of internally mixed BC (cf. Fig. S5). For this, the absorption enhancement,  $E_{abs}$  attributed to the different values of AAE for the internally mixed BC can be described as follows (Eq. 3):

$$E_{abs,int}^{\lambda} = 1 + \frac{MAC_{BC,int}^{880\text{nm}} \cdot \left(\frac{880}{\lambda}\right)^{\text{AAE}}}{MAC_{ref}^{\lambda}}, \quad (3)$$

where for the sensitivity study presented here, different AAE (0.8, 1 and 1.4) were considered following Lack and Langridge 225 (2013).

Finally, the absorption enhancement due to externally mixed particles at a given wavelength,  $E_{abs,ext}^{\lambda}$ , was obtained as the difference between the measured total ambient absorption enhancement and the absorption enhancement due to the internal mixing,

$$E_{abs,ext}^{\lambda} = E_{abs}^{\lambda} - E_{abs,int}^{\lambda}. \quad (4)$$

## 230 2.5 Chemical fractions contribution to $E_{abs}$

Submicron chemical composition from ACSM in BCN and offline 24h chemical speciated data from filter analyses at both BCN and MSY were used to determine the influence of the material available for BC coating on  $E_{abs}$ . Chemical speciated data were used to calculate the total amount of non-refractory particulate matter (NR-PM<sub>10</sub> for offline measurements and NR-PM<sub>1</sub> for online measurements) mass concentration. The NR-PM to EC concentration ratios were then calculated as follows:

$$235 \quad R_{NR-PM} = \frac{\sum_i [NR-PM]_i}{[EC]}; \quad (5)$$

Thus, the calculated  $R_{NR-PM}$  represents a proxy for the amount of non-refractory material available for mixing with the BC particles (Cappa et al., 2019). The chemical species and groups of compounds taken into account using the online ACSM continuous measurements were:  $[HOA]$ ,  $[COA]$ ,  $[LO-OOA]$ ,  $[MO-OOA]$ ,  $[SO_4^{2-}]$ ,  $[NO_3^-]$ ,  $[NH_4^+]$  and  $[Cl^-]$ , plus  $[BBOA]$  during the cold period; whereas from the 24-hour filters they were:  $[OA]$ ,  $[SO_4^{2-}]$ ,  $[NO_3^-]$ ,  $[NH_4^+]$ ,  $[Cl^-]$ .

240 Moreover, online submicron chemical composition data and OA source apportionment from ACSM in BCN were used to determine the species that mostly contributed to  $E_{abs}$ . For this, a multivariate linear regression (mlr) analysis was employed to solve the following equation:

$$E_{abs} = E_0 + m_1[q_1] + m_2[q_2] + \dots + m_z[q_z]; \quad (6)$$

where  $E_0$  is the intercept,  $m_i$  (where  $i = 1, \dots, z$ ) are the regression coefficients, i.e. the relative contribution of each chemical fraction to  $E_{abs}$ , and  $[q_i]$  are the dependent variables of the mlr, i.e. the ratios of each chemical fraction/source normalized to the EC concentration. Note that  $E_0$  should be equal to 1 (i.e. no absorption enhancement) when all the ratios are equal to 0 in eq. (6). In order to perform a more robust mlr analysis and to reduce the effect of outliers, data points lower than the 5th and higher than the 95th percentiles were excluded from the analysis.

### 3 Results

#### 250 3.1 Site specific MAC and $E_{abs}$ analysis

The median values of the ambient BC MAC and  $E_{abs}$  at different wavelengths from both online and offline measurements at BCN and MSY are reported in Table 1 and Table 2, respectively. For the long-term offline measurements, the MAC at 637 nm was  $9.67 \pm 2.55 \text{ m}^2 \text{g}^{-1}$  at BCN urban background station, and  $13.10 \pm 4.47 \text{ m}^2 \text{g}^{-1}$  at MSY regional background station. The BC MAC at MSY showed a higher median value compared to BCN (cf. Table 1) due to the fact that BC particles reaching the 255 regional station had more time to gather material for coating. Moreover, the frequency distribution of the MAC values at MSY was less left-skewed and more right-skewed compared to BCN (see Fig. S7). For the intensive online measurements in BCN, the MAC ranges between  $7.55 \pm 2.06$  at 950 nm and  $22.74 \pm 6.98$  at 370 nm (Table 1). The values at 660 nm for the online measurements and 637 nm for the offline measurements were around  $10.85 \pm 2.98$ , and  $9.67 \pm 2.55$  in BCN, and  $13.10 \pm 4.47$  in MSY, which were within the range of MAC values reported by Zanatta et al. (2016) for similar station backgrounds. The 260 difference between the offline and online measurements at BCN, although the mean values fall within the standard deviation of the measurements, was mainly associated to the difference in the length of the measurement periods, and the different inlet cut-offs (Fig. S1). The observed increase of MAC with decreasing wavelength was expected due to both the increase of the energy radiation and the larger influence of the externally mixed BrC particles at shorter wavelengths. In fact, the effect on MAC of externally mixed BrC particles in BCN is visible in Fig. S7 where the frequency distribution of MAC at 370 nm 265 showed a much more pronounced tail toward higher values compared to the MAC at 880 nm.

**Table 1.** Observed MAC ( $\text{m}^2 \text{g}^{-1}$ ) values obtained using online techniques via AE33 and Sunset online EC measurements at BCN ( $\text{BCN}_{\text{on}}$ ), and offline at BCN and MSY via MAAP and offline EC measurements on 24-hour filters ( $\text{X}_{\text{off}}$ ).

	$\lambda \text{ (nm)}$	MAC
<b>Online BCN</b>	<b>370</b>	$22.74 \pm 6.98$
	<b>470</b>	$17.23 \pm 4.80$
	<b>520</b>	$14.84 \pm 4.16$
	<b>590</b>	$12.63 \pm 3.50$
	<b>660</b>	$10.85 \pm 3.02$
	<b>880</b>	$7.92 \pm 2.16$
	<b>950</b>	$7.55 \pm 2.06$
<b>Offline BCN</b>	<b>637</b>	$9.67 \pm 2.55$
<b>Offline MSY</b>	<b>637</b>	$13.10 \pm 4.47$

The averaged multi-wavelength absorption enhancement values from both online and offline measurements at BCN and MSY are shown in Table 2. The online measurements at 880 nm in BCN led to a median value of  $E_{abs}$  of  $1.28 \pm 0.36$ , whereas

it increased to  $1.45 \pm 0.51$  at 370 nm. For the offline measurements, the median  $E_{abs}$  values at 637 nm were  $1.42 \pm 0.40$  and  $2.00 \pm 0.75$  at BCN and MSY, respectively. As reported in Table 2, the  $E_{abs}$  values from online and offline measurements in BCN were rather similar ( $1.31 \pm 0.38$  at 660 nm online and  $1.42 \pm 0.40$  at 637 nm offline), and the observed difference was likely due to both the different periods, the inlet cut-off (Fig. S1) and the different instrumentation used for the calculation of  $E_{abs}$ . As already observed for the MAC, the higher  $E_{abs}$  at the regional MSY station was due to ageing of BC particles during the transport toward the regional station. The  $E_{abs}$  reported in Table 2 were calculated from eq. (2) using as  $MAC_{ref}^{\lambda}$  the intercept values from the Deming regression fits reported in Figs. S2-S4,S6 for online AE33 and offline BCN and MSY, respectively. If the theoretical reference MAC (Bond and Bergstrom, 2006) of uncoated BC was used, the overall median  $E_{abs}$  values were higher for the online measurements at BCN ( $1.59 \pm 0.51$  at 880 nm and  $1.91 \pm 0.62$  for 370 nm), although within the uncertainty, and rather similar for the offline measurements at BCN and MSY, with  $E_{abs}$  values at 637 of  $1.43 \pm 0.44$  and  $1.92 \pm 0.76$ , respectively (Table 2). The values found at the urban BCN area using the experimental (theoretical) reference MAC at 880 nm were similar (higher) to those observed in the literature for the same wavelength at rural/suburban areas (Liu et al., 2015; Zhang et al., 2018). The mean  $E_{abs}$  value observed at the regional background MSY station was also similar to the values reported in literature for rural areas (e.g., Cui et al., 2016).

**Table 2.** Overall, and cold and warm period average  $E_{abs}$  values for both multi-wavelength online measurements at BCN, and offline measurements at the near-infrared at BCN and MSY station.

$\lambda$ (nm)	$E_{abs,exp}$			$E_{abs,theory}$			
	Overall	cold	Warm	Overall	cold	Warm	
<b>Online BCN</b>	<b>370</b>	$1.45 \pm 0.51$	$1.67 \pm 0.57$	$1.31 \pm 0.35$	$1.91 \pm 0.69$	$2.11 \pm 0.79$	$1.79 \pm 0.53$
	<b>470</b>	$1.38 \pm 0.43$	$1.53 \pm 0.50$	$1.27 \pm 0.29$	$1.85 \pm 0.61$	$2.00 \pm 0.71$	$1.76 \pm 0.45$
	<b>520</b>	$1.35 \pm 0.41$	$1.47 \pm 0.48$	$1.27 \pm 0.30$	$1.76 \pm 0.58$	$1.91 \pm 0.67$	$1.67 \pm 0.43$
	<b>590</b>	$1.33 \pm 0.39$	$1.42 \pm 0.46$	$1.27 \pm 0.29$	$1.70 \pm 0.55$	$1.83 \pm 0.65$	$1.61 \pm 0.40$
	<b>660</b>	$1.31 \pm 0.38$	$1.39 \pm 0.45$	$1.26 \pm 0.29$	$1.63 \pm 0.54$	$1.76 \pm 0.63$	$1.55 \pm 0.39$
	<b>880</b>	$1.28 \pm 0.36$	$1.33 \pm 0.43$	$1.25 \pm 0.28$	$1.59 \pm 0.51$	$1.69 \pm 0.60$	$1.52 \pm 0.37$
	<b>950</b>	$1.28 \pm 0.36$	$1.33 \pm 0.43$	$1.25 \pm 0.28$	$1.59 \pm 0.51$	$1.69 \pm 0.60$	$1.52 \pm 0.37$
<b>Offline BCN</b>	<b>637</b>	$1.42 \pm 0.40$	$1.41 \pm 0.39$	$1.45 \pm 0.40$	$1.43 \pm 0.44$	$1.42 \pm 0.43$	$1.43 \pm 0.44$
<b>Offline MSY</b>	<b>637</b>	$2.00 \pm 0.75$	$1.82 \pm 0.63$	$2.24 \pm 0.79$	$1.92 \pm 0.76$	$1.73 \pm 0.66$	$2.02 \pm 0.81$

Figure 1 shows the density distribution of  $E_{abs}$  for the cold (from December to May) and warm (from June to October) seasons from both online measurements at BCN and offline measurements at BCN and MSY (Fig. 1). The median values of the season-dependent frequency distributions of  $E_{abs}$  were reported in Table 2. The long-term offline measurements led, on average, to similar  $E_{abs}$  values at 637 nm in BCN during the warm ( $1.45 \pm 0.40$ ) and cold ( $1.41 \pm 0.39$ ) seasons. However, at MSY  $E_{abs}$  values were larger during the warm period ( $2.24 \pm 0.79$ ) compared to the cold period ( $1.82 \pm 0.63$ ), mainly due to

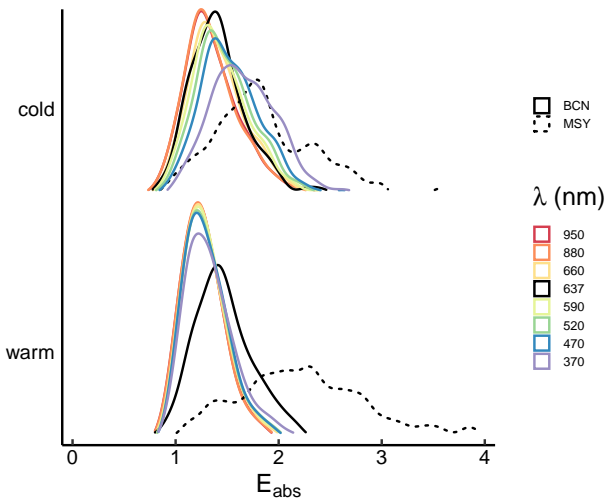


**Figure 1.** Seasonal frequency distributions of  $E_{abs}$  at BCN for the multiple wavelengths measured with the AE33 (colored solid lines for 370, 470, 520, 590, 660, 880 and 950 nm), and at BCN (black solid line) and MSY (black dash line) measured with a MAAP 637 nm and offline filters.

the increase in the secondary organic aerosol formation (Figs. S8 and S9) which was mostly driven by the increase in biogenic volatile organic compounds (VOCs) during the warm season (Seco et al., 2013; Veld et al., 2021). Thus, as shown later in more detail, OA, and especially SOA, contributed strongly to the BC lensing-driven absorption enhancement, especially at the

290 regional station.

The online measurements performed with AE33 aethalometer allowed for a multi-wavelength analysis of  $E_{abs}^\lambda$ . Figure 1a shows a seasonal decoupling of  $E_{abs}$  between the near-ultraviolet and the infrared wavelengths: whilst in the warm period  $E_{abs}$  remained similar for all the wavelengths, during the cold period there was an increase of  $E_{abs}$  towards the shorter wavelengths. This different amplification of the absorption enhancement at the near-ultraviolet can be associated with a larger presence of 295 BrC-like compounds (e.g. BBOA from winter biomass burning) (Figs. S8 and S9) during the cold period (Via et al., 2021), which present larger mass absorption cross-sections and contribution to absorption at these wavelength range (e.g. Lack et al., 2012; Qin et al., 2018; Saleh et al., 2018; Saleh, 2020; Kasthuriarachchi et al., 2020; Zhang et al., 2020). Figure S10 shows that by using the theoretical reference MAC the density distribution of  $E_{abs}$  was similar, although the differences between the cold and warm period were not that great. This was attributed to the fact that using a theoretical MAC does not take into account 300 the different seasonal-dependent contributions of OA sources.

### 3.1.1 $E_{abs}$ dependence on the mixing state

As already stated, ambient BC particles can be either externally or internally mixed with other aerosols (Bond and Bergstrom, 2006). In order to separate the relative contributions to  $E_{abs}$  of these two mixing states, i.e. external ( $E_{abs,ext}$ ) and internal

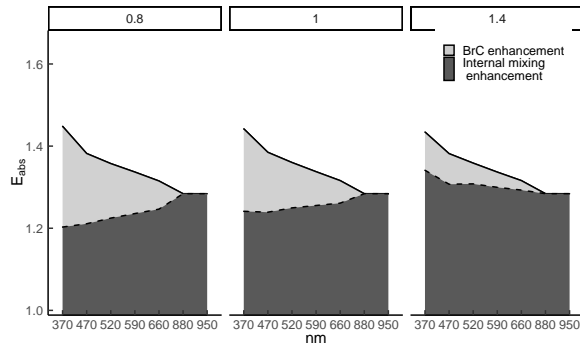


**Figure 2.** Absorption enhancement,  $E_{abs}$ , attribution to both internal and external mixing under different AAE conditions for the internally mixed BC (0.8,1,1.4) for the online measurements at the 7-AE33 wavelengths at Barcelona (BCN).

( $E_{abs,int}$ ), we used the multi-wavelength AE33 and the semi-continuous OC:EC measurements obtained in BCN (see Sect.

305 2.4). We assumed that the  $E_{abs}$  at the near-infrared (880 nm) was only produced by the internal mixing of BC particles, whereas at the short-UV (370 nm) the  $E_{abs}$  is due to both the internal and external mixing of BC particles. Given the spectral characteristic of BrC absorption, the contribution to  $E_{abs}$  due to external mixing was the highest at 370 nm compared to the other AE33 wavelengths. In addition, here we analyzed the possible contribution of different internal mixing states of BC using different AAE for internally mixed BC, since the presence of brown coatings over the BC cores can actually produce a 310 reduction of the enhancement of the absorption towards the shorter wavelengths (cf. Lack and Cappa, 2010).

Figure 2 shows the evolution of the contribution of the internal and the external mixing to the total  $E_{abs}$  for the three AAE values considered for internally mixed BC. Indeed, Fig. 2 shows that an AAE of 0.8 could be related with a larger proportion of brown coatings reducing the absorption enhancement due to the internally mixed BC (cf. Fig. 5 Lack and Cappa, 2010). In the case of AAE=1, the contribution of the coating material remains fairly constant (Fig. 2), although it presents a slight decrease 315 with decreasing wavelengths, which is due to the fact the MAC Ångström Exponent presented here for the experimental reference MAC for pure BC particles was slightly above 1 (Fig. S6). Moreover, Fig. 2 shows that for an AAE of 1.4 the internal mixing increases towards the shorter wavelengths, as observed in the simulations performed in Fig. 3 of Lack and Cappa (2010) for the case of BC core with a brown shell that does not absorb.

The overall contribution due to the internal mixing ( $E_{abs,int}$ ) ranged between a 100% at 880 nm, and 83, 86, and 93.5% 320 of the total  $E_{abs}$  at 370 for an AAE of 0.8, 1 and 1.4, respectively. Thus, the BrC externally mixed particles represented a non-negligible fraction of the total  $E_{abs}$  at near-ultraviolet wavelengths (Table S1), especially for the AAE=0.8 case, for which it increased from  $0.069 \pm 0.066$  (5.2%) at 660 nm up to  $0.17 \pm 0.18$  at 370 nm (16.9%). Conversely, if an AAE=1.4 is used, then the increase and relative contribution of  $E_{abs}$  due to the BrC externally mixed particles remains lower, from  $0.023 \pm 0.049$  (1.7%) at 660 nm up to  $0.093 \pm 0.200$  at 370 nm (6.5%).

325 Although BCN is an urban background station with a non-predominant contribution from biomass burning, the contribution to absorption from other potential BrC sources cannot be excluded. Since biomass burning emissions are higher during the cold

season, we have found that during this season compared to the warm period there was a small increase of the total absorption enhancement due to the internal mixing (6.4%), and a more significant increase of contribution of the external mixing  $E_{abs}$ , which increased for an AAE=1 from 0.09 during the warm period to 0.36 during the cold season (Table S1 and Fig. S11), i.e. 330 from representing a 7% to 22% of the total  $E_{abs}$ , respectively. In fact, biomass burning is not the only source contributing to the presence of BrC in the atmosphere during the colder months (e.g. Zhang et al., 2020), in fact, as shown later, other OA sources also contribute to  $E_{abs}$ .

### 3.2 $E_{abs}$ dependence on $R_{NR-PM}$ content

Here we analyzed the relationship between the  $E_{abs}$  and the amount of material available for mixing with BC particles 335 ( $R_{NR-PM}$ , c.f. Sect. 2.5). As commented in Sect. 3.1, the variability of  $E_{abs}$  with the seasons can be attributed to the differences in the OA composition and concentration levels. Cappa et al. (2019) have shown the discrepancies between model, laboratory and field studies in the behaviour of  $E_{abs}$  with  $R_{NR-PM}$ . Indeed, Figure 1 in Cappa et al. (2019) shows that some 340 studies reported only a slight increase of  $E_{abs}$  with the amount of the coating material (Cappa et al., 2012), whereas others measured a larger increase of  $E_{abs}$  for high concentrations of  $R_{NR-PM}$  (Liu et al., 2015; Peng et al., 2016). The authors argued that the differences could be associated to the ageing state, volatility, and amount of coating of the particles, as well as to the apportionment of external mixing to  $E_{abs}$ .

Figure 3 shows  $E_{abs}$  values as a function of  $R_{NR-PM}$  at BCN (online and offline) and MSY (offline). Overall, we observed an exponential increase of the absorption enhancement with the amount of NR-PM coating material available for mixing (Fig. 3), which was consistent with some of the observed behaviour found in the literature (e.g. Fig. 1 in Cappa et al., 2019).

345 As shown in Fig. 3, the  $R_{NR-PM}$  binned values from offline measurements at MSY spanned from around 15 up to around 55  $\mu\text{g}/\text{m}^{-3}$ , whereas in BCN  $R_{NR-PM}$  values were between around 3.5 and 20  $\mu\text{g}/\text{m}^{-3}$ . As a consequence, the  $E_{abs}$  at MSY reached values up to around 3.25, whereas in BCN  $E_{abs}$  values remained lower than 2. Thus, the higher  $R_{NR-PM}$  at MSY implied that more material was available for BC coating at the regional site compared to BCN, thus leading to higher  $E_{abs}$  at 350 MSY. Moreover, the lowest  $E_{abs}$  at MSY from binned data in Fig. 3 was around 1.3 indicating that on average BC particles reaching MSY station have undergone a longer aging processes and were already coated, whereas in BCN freshly emitted still-not-mixed BC particles were frequently measured, as denoted by  $E_{abs}$  values closer to 1. For the online measurements in BCN,  $R_{NR-PM}$  showed a larger range of values (from around 4 to 40  $\mu\text{g}/\text{m}^{-3}$ ) compared to the offline measurements because of the higher time resolution of on-line measurements allowing measuring events characterized by lower or higher  $R_{NR-PM}$  compared to the 24-hour offline measurements. The higher  $E_{abs}$  in BCN at 637 nm compared to  $E_{abs}$  at 370 nm was 355 mostly associated to the different inlets size cut-offs and, to a lesser extent, to the different periods used for the online and offline measurements. In fact, as shown in Fig. S12, the mean  $E_{abs}$  calculated from offline measurements in BCN using the same period as for the online measurements (2018) was closer to the  $E_{abs}$  values obtained from online measurements at 880 nm and 370 nm. As shown in Fig. 3, the  $E_{abs}$  values from the online and offline datasets in BCN, showed similar trends for smaller concentrations of  $R_{NR-PM}$ . However, as the amount of mixing material increased, the offline method increased at a 360 higher rate, reaching higher values for the largest  $R_{NR-PM}$  measurements. This behaviour was also observed when only the

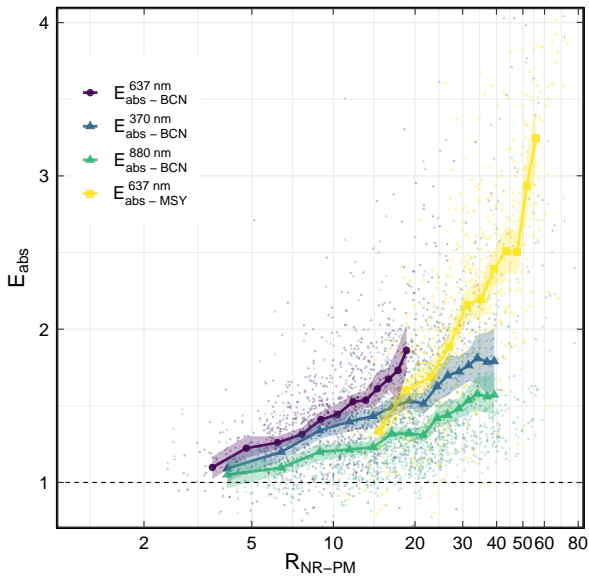


**Figure 3.** Absorption enhancement,  $E_{\text{abs}}$ , as a function of the non-refractory PM to EC ratio at both Barcelona (BCN) and Montseny (MSY) station. The offline  $E_{\text{abs}}$  measurements with a  $\text{PM}_{10}$  inlet at 637 nm were used for both BCN and MSY. Also, at BCN, online  $E_{\text{abs}}$  measurements with a  $\text{PM}_{2.5}$  inlet at the short-UV (370 nm) and near-IR (880 nm) wavelengths were used. The scatter points represent all the measurements, whereas the marked points show the mean of each bin, whilst the shadow of the line represent the standard deviation of each bin.

2018 year period was used for the calculation of  $E_{\text{abs}}$  from offline measurements (cf. Fig. S12). These different trends between online and offline  $E_{\text{abs}}$  versus  $R_{\text{NR-PM}}$  were probably due to two main factors: first, the offline measurements were made with a  $\text{PM}_{10}$  inlet vs the  $\text{PM}_{2.5}$  inlet of the online method (Fig. S1), hence coarse nitrates and other coarse particles could have influenced  $E_{\text{abs}}$ , and, second, the large annual variability observed for the offline  $E_{\text{abs}}$  measurements (see Fig. S12) could have 365 also contributed to the observed difference.

The availability of multiple wavelength absorption enhancement values at BCN station allowed a multi-wavelength analysis of  $E_{\text{abs}}$  versus  $R_{\text{NR-PM}}$ . Since  $E_{\text{abs}}$  at 880 nm is influenced solely by the internal mixing of BC particles, the comparison of  $E_{\text{abs}}$  at 880 nm and 370 nm, when the external mixing influence on the absorption is the highest, showcased the influence that the mixing state had on the relationship between  $E_{\text{abs}}$  and  $R_{\text{NR-PM}}$ . Figure 3 shows similar values for both wavelengths 370 for the lowest amount of coating material, but as  $R_{\text{NR-PM}}$  increased the absorption enhancement at 370 nm increased more rapidly than at 880 nm, mostly due to the fact that as  $R_{\text{NR-PM}}$  increases the contribution of BrC externally mixed becomes larger.

If a theoretical MAC reference was used instead, the  $E_{\text{abs}}$  values as a function of  $R_{\text{NR-PM}}$  at BCN (online and offline) and MSY (offline) showed the same relationship (Fig. S13), albeit larger values were observed, specially for the AE33 measure-

**Table 3.** Multivariate linear regression analysis coefficients and standard deviation of the chemical fraction influence on the absorption enhancement,  $E_{abs}$ , for Barcelona at both 370 and 880 nm wavelengths using the Q-ACSM chemical sources (Via et al., 2021)

	370 nm		880 nm	
	Cold	Warm	Cold	Warm
<b>Intercept</b>	1.097 ± 0.062	1.112 ± 0.028	1.003 ± 0.048	1.109 ± 0.022
<b>HOA:EC</b>	0.195 ± 0.099	0.092 ± 0.038	0.126 ± 0.077	0.019 ± 0.029
<b>BBOA:EC</b>	0.175 ± 0.058		-0.062 ± 0.044	
<b>MO-OOA:EC</b>	0.044 ± 0.021	0.010 ± 0.007	0.040 ± 0.016	-0.009 ± 0.005
<b>LO-OOA:EC</b>	0.161 ± 0.064	-0.001 ± 0.006	-0.012 ± 0.049	0.006 ± 0.005
<b>Sulphate:EC</b>	-0.003 ± 0.017	0.010 ± 0.004	0.012 ± 0.013	0.017 ± 0.003
<b>Nitrate:EC</b>	-0.011 ± 0.010	0.087 ± 0.011	-0.006 ± 0.008	0.060 ± 0.009
<b>COA:EC</b>	0.106 ± 0.040	0.032 ± 0.022	0.035 ± 0.030	0.044 ± 0.018

375 ments. These larger values were mostly due to the fact that the experimentally used MAC was higher than the theoretical ones (Fig. S6), resulting in larger  $E_{abs}$  values (Fig. S13).

### 3.3 Aerosol sources contribution to $E_{abs}$

380 The material available for coating on BC particles, which determines its absorption enhancement properties (see Fig. 3), is formed by an array of different chemical compounds from different sources as a result of a succession of physical and chemical processes in the atmosphere. These different chemical compounds can exert different responses on  $E_{abs}$  (e.g. Zhang et al., 2018) and can increase the BC  $E_{abs}$  depending on their relative amount compared to BC as shown in Fig. 3 and the literature (Zhang et al., 2018; Cappa et al., 2019, and therein).

385 Here we analyzed the contribution of different OA sources and chemical species, as sulphate and nitrate, to the  $E_{abs}$  calculated in Barcelona from online measurements via a multi-variate linear regression analysis. The OA sources were obtained by means of a PMF analysis on the Q-ACSM data in BCN and were published by Via et al. (2021). Given the differences in the seasonality that the OA sources can present, as also observed in BCN (cf. Fig. S9; Minguillón et al., 2015; Via et al., 2021), and given the observed  $E_{abs}$  seasonality (Fig. 2), we applied the MLR analysis separately to the warm and cold periods. Furthermore, in order to separate the contribution of the different BC mixing states, we performed the mlr analyses at the same wavelengths as in Sect. 3.2, namely 370 and 880 nm.

390 The results of the mlr analysis were reported in Table 3. Table 3 shows that overall, regardless of the season and the wavelength considered, the main contributors to  $E_{abs}$  in BCN were Hydrocarbon-like OA (HOA), associated to the emissions from traffic, and cooking-related OA (COA). These two sources contributed 12 and 14 %, respectively, to the measured OA mass concentration (Via et al., 2021). Thus, in BCN, HOA and COA increased  $E_{abs}$  both by contributing to the BC coating (880 nm)

and by acting as BrC species externally mixed with BC (370 nm), as suggested by the higher coefficients observed for these  
395 two OA sources at 370 nm compared to 880 nm (cf. Table 3). A major source of BC in BCN was traffic (Pandolfi et al., 2016;  
Via et al., 2021), thus likely explaining the high potential of HOA particles to contribute to  $E_{abs}$ . Moreover, some recent  
studies have also shown that HOA particles in urban environments can potentially have a high absorption efficiency in the  
UV-VIS (Qin et al., 2018; Chen et al., 2020; Kasthuriarachchi et al., 2020). Regarding the COA particles, some studies have  
400 shown that this OA source has a lower absorption efficiency compared to HOA particles (e.g. Qin et al., 2018; Kasthuriarachchi  
et al., 2020; Chen et al., 2020). This was in agreement with the lower coefficients observed for COA compared to HOA  
(Table 3). In addition, during the cold period both BBOA and LO-OOA presented large positive contributions to  $E_{abs}$  at 370  
nm, whereas at 880 nm the contribution to  $E_{abs}$  from these two sources was negative. For the warm period the contribution of  
LO-OOA was also very low at 880 nm and negative at 370 nm whereas, as already stated BBOA did not contribute in summer.  
Zhang et al. (2018) also found a negative contribution to  $E_{abs}$  for BBOA at 880 nm. The higher coefficients observed for these  
405 sources (HOA, COA, BBOA and LO-OOA) at 370 nm compared to 880 nm highlighted the potential of these OA sources to  
act as BrC species externally mixed with BC. MO-OOA particles also contributed positively to  $E_{abs}$  at both 370 nm and 880  
nm especially during the cold season likely due to the higher relative contribution of MO-OOA to OA observed in this season  
compared to the warm period (Via et al., 2021). Recently, Kasthuriarachchi et al. (2020) reported higher absorption efficiency  
410 in the UV-VIS range for LO-OOA particles compared to MO-OOA particles likely due to the photo-degradation chemistry  
(photo-bleaching) of BrC chromophores in this aged MO-OOA fraction. The inorganic aerosol components presented a higher  
variability with regards to their contribution to  $E_{abs}$ , with sulphates, and especially nitrates, becoming an important source of  
coating during the warm period, whilst presenting a low impact during the colder period.

Figure 4 shows the contribution to  $E_{abs}$  from the OA sources and inorganic species included in the mlr analysis as  $R_{NR-PM}$   
increases. The contributions to  $E_{abs}$  reported in Figure 4 were calculated as the product between the OA sources and inorganic  
415 species mass concentrations (provided by Via et al., 2021) to EC ratios and the coefficients reported in Table 3. As shown in Fig.  
4, during the cold season in BCN the absolute contribution of OA to  $E_{abs}$  was much higher compared to the contribution from  
inorganic aerosols (nitrates and sulphates here) at both 370 nm and 880 nm (Figs. 4a,c). HOA and MO-OOA were the major  
sources contributing to the lensing-driven absolute BC absorption enhancement at 880 nm in BCN during the cold season.  
Conversely, the absolute contribution of LO-OOA and COA to  $E_{abs}$  was the highest at 370 nm suggesting their importance as  
420 BrC source in the area under study. During the warm period, as already noted,  $E_{abs}$  was lower compared to the cold period.  
The major difference compared with the cold period was that the contribution of secondary inorganic aerosols increased. It was  
notable the contribution at 880 nm of sulphates as BC lensing-driving species. Furthermore, Fig. 4 also shows that when the  
contributions were negative, these did not have a large effect upon the overall  $E_{abs}$ .

### 3.4 Atmospheric aging influence on $E_{abs}$

425 Atmospheric aging and oxidation of OA particles have been shown to have an important effect on the absorption enhancement  
(e.g., Liu et al., 2015; Zhang et al., 2018; Xu et al., 2018; Wu et al., 2018). Indeed, we have shown that the SOA (LO-OOA +  
MO-OOA) were the main contributors to  $E_{abs}$  during the cold period (Table 3 and Fig. 4).

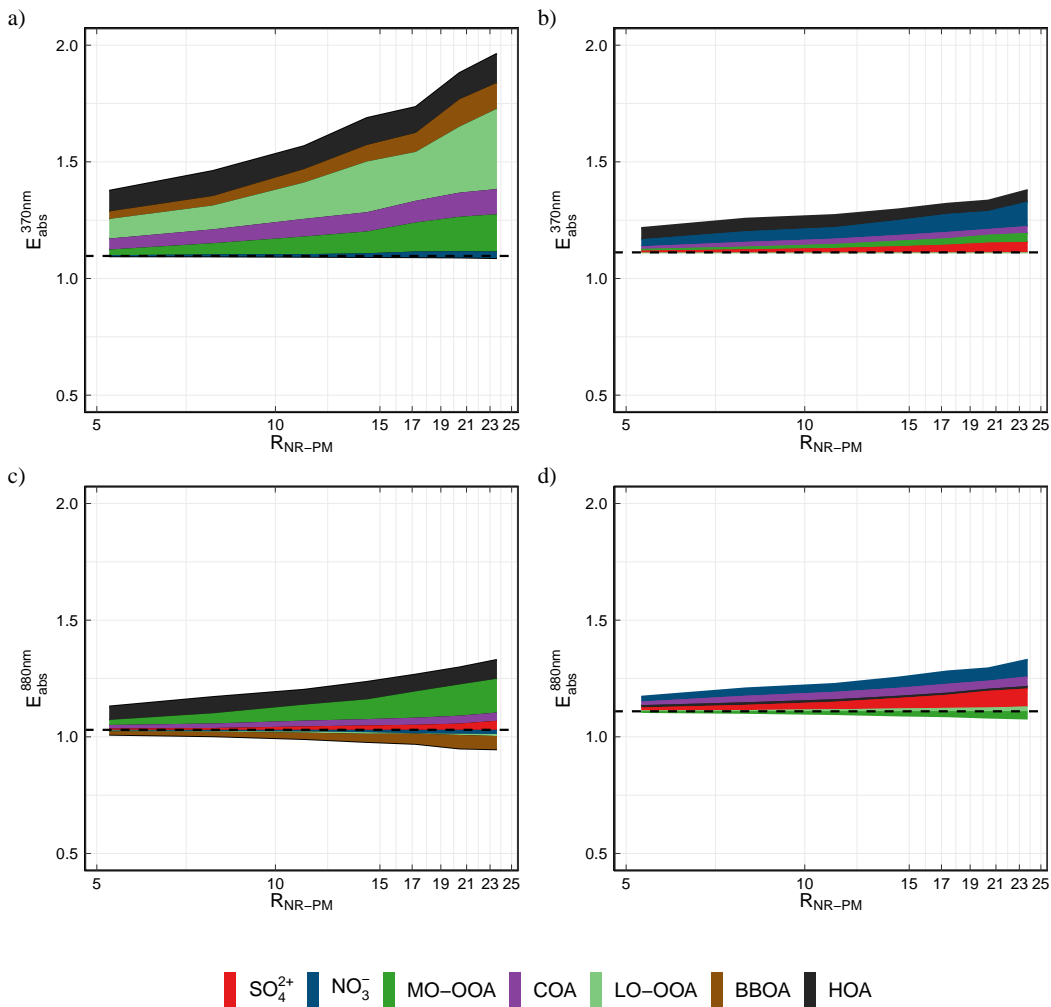


**Figure 4.** Contribution to the absorption enhancement,  $E_{\text{abs}}$  as a function of the amount of coating material  $R_{\text{NR-PM}}$  for the different organic and inorganic sources found at BCN during the cold period (left panel) and warm period (right panel) for 370 (upper panel) and 880 nm (lower panel). The contribution for each source was computed by applying the coefficient obtained with the mlr analysis (see Table 3) to the ratio that that compound-to-EC had as  $R_{\text{NR-PM}}$  increased. It should be noted that for each season and wavelength, we have set the corresponding intercept of the mlr analysis as reference value above/below which each compound presented a positive/negative influence on  $E_{\text{abs}}$ .

Here we studied the behaviour of the absorption enhancement with the aging state of the aerosols. With this aim, we followed the visual method proposed by Ng et al. (2010) to characterize the aging state of the particles, the so-called triangular plot, 430 where the y-axis shows the  $f_{44}$  factor (mz/44 to total concentration in the ACSM component mass spectra ratio), which is a proxy of the aging, and the x-axis is the  $f_{43}$  factor (mz/43 to total concentration in the component mass spectra ratio), which

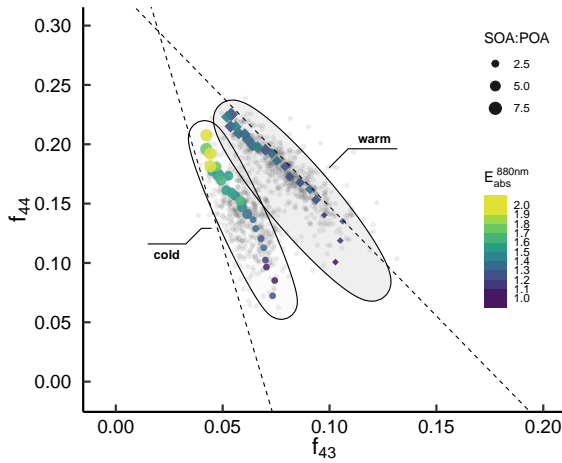


**Figure 5.** Absorption enhancement,  $E_{abs}$ , at 880 nm at BCN using online measurements as a function of the primary to secondary organic aerosol ratio (POA:SOA), and the atmospheric aging (following Ng et al. (2010) proposed triangle plot,  $f_{44}$  vs  $f_{43}$ ). The  $f_{44}$  and  $f_{43}$  factors used are the ones presented by Via et al. (2021) for the same time period from the Q-ACSM measurements.

shows the differences in the sources and chemical pathways for OOA formation. As particles become more oxidized they converge towards higher  $f_{44}$  values and lower  $f_{43}$  values.

As observed in Table 3 and Fig. 4 overall primary sources such as HOA, COA and BBOA were important drivers of the absorption enhancement, although SOA sources, especially during the cold period and for the shorter wavelengths, were also important sources contributing to  $E_{abs}$ . Figure 5 shows the  $f_{44}$ - $f_{43}$  relationship in BCN as a function of both  $E_{abs}$  values at 880 nm, where  $E_{abs}$  is driven by the lensing effect, and the SOA:POA ratio. Figure 5 shows a clear separation of the  $f_{44}$ - $f_{43}$  relationship between the cold and warm periods. In fact, during the cold period at 880 nm, as aerosols become more oxidized (higher  $f_{44}$ ), the SOA:POA ratio increased altogether with an increase of the absorption enhancement. Conversely, during the warm period, although the SOA:POA ratio also increased with the degree of oxidation, the absorption enhancement did not increase significantly. Therefore, during the cold period as particles became more oxidized, BC particles internally mixed with SOA (mainly MO-OOA as shown in Fig. 4c) were the main responsible for the larger  $E_{abs}$  values, whereas during the warm period, since the main drivers of  $E_{abs}$  were the inorganic compounds (Fig. 4d) higher  $f_{44}$  values did not imply an increase in  $E_{abs}$ . Furthermore,  $E_{abs}$  at 370 nm (see Fig. S14) during the cold period showed a more pronounced increase as particles became more oxidized, mainly due to the role of externally mixed BrC, which, as reported in Fig. 4 were the main contributors to  $E_{abs}$ . Fig. S14 showed that  $E_{abs}$  at 370 nm during the warmer period presented a slight increase as particles became oxidized, which could be attributed to the small contribution that MO-OOA particles exerted during this period (see Fig. 4b). This tendency toward higher  $E_{abs}$  values as particles become more oxidized has also been found in Paris by Zhang et al. (2018), and in London by Liu et al. (2015).

450 3.5  $E_{abs}$  trend analysis

As already stated, the average  $E_{abs}$  values obtained by the offline method at BCN and MSY at 637 nm were within the values found in the literature for similar urban/regional background stations. Given the impact that the absorption enhancement of BC particles has on climate, we performed a seasonal trend analysis of  $E_{abs}$  at both BCN (from 2011 to 2020), and MSY (from 455 2010 to 2020). In this trend analysis, as well as for the other results presented in this work, we excluded the days when Saharan dust outbreaks influenced the measurements to avoid UV absorption by dust in the analyses presented. Moreover, as already stated, the trend analysis was performed on  $E_{abs}$  calculated at 637 nm, where the contribution to  $E_{abs}$  from externally mixed OA was less relevant.

The method employed for the trend analysis was a Theil-Sen slope regression estimator. Previous studies performed at MSY and BCN have shown statistically significant (s.s) decreasing trends over time for the contributions from various anthropogenic 460 sources including traffic, industry, heavy-oil combustion, secondary sulphate and secondary nitrates mirroring the success of mitigation strategies adopted in Europe (Pandolfi et al., 2016; Veld et al., 2021). Moreover, recently (Veld et al., 2021) have shown that the observed decreasing trends, in combination with the absence of a trend for the organic aerosols (OA) at both BCN and MSY, resulted in an increase in the relative proportion of OA in PM at these stations, and especially for the SOA, which presents the higher values during the summer season.

465  $E_{abs}$  trends showed different behaviours during spring-summer and autumn-winter periods at the two urban and background stations considered here (Fig. 6). Figure 6 shows a s.s. increase of  $E_{abs}$  at MSY summer (JJA), whereas no s.s. trends were observed at MSY during the other seasons. In BCN the  $E_{abs}$  trends were no s.s. during all the seasons. During autumn (SON) and winter (DJF),  $E_{abs}$  showed a slight decrease at both stations although not s.s. The  $E_{abs}$  s.s. increase of a 8.16 % per year during summer at MSY was linked to the observed increase of the OC:EC ratio (cf. Fig. S15), thus further confirming the 470 importance of OA particles to form internal mixing with BC particles, thus increasing the  $E_{abs}$ . Conversely, the sulphate:EC ratio (Fig. S16) did not show any seasonal s.s. trend at both sites, mostly because both sulphates and EC concentrations decreased during the period under study (cf. Pandolfi et al., 2016; Veld et al., 2021). The observed OC:EC ratio increase at MSY in summer was mainly driven by the increase in the relative proportion of SOA particles as shown in (Veld et al., 2021). We have shown here that as the aerosols become more oxidized the SOA:POA ratio increased together with  $E_{abs}$  and 475 the OC:EC s.s. trend observed further confirmed the importance of aged OA particles to form BC coating. In the case that the theoretical MAC was used as a reference (Bond and Bergstrom, 2006), the  $E_{abs}$  showed the same behaviour with an increase at the regional station, MSY, during the summer months (Fig. S17).

480 During MAM of 2020 there was a notable  $E_{abs}$  increase at both stations, and especially in BCN. During this period, a strict lockdown was established in Spain due to restrictions under the COVID-19 pandemic. The strict lockdown measures implied a significant decrease in the emission of BC and primary aerosols due to the orders to halt any non-essential activity (Tobías et al., 2020; Evangelou et al., 2021; Querol et al., 2021). This decrease in the primary emissions resulted in an increase in the OC:EC ratio, as can be appreciated in Fig. S15a, which can be associated with an increase in  $E_{abs}$ .

The observed changing behaviour of  $E_{abs}$  under different SOA:POA ratios suggested that the absorption enhancement may undertake changes, and possibly an increase, upon new emission restrictions. In fact, as already stated and as shown in Veld 485 et al. (2021) an increase in the relative proportion of OA in  $PM_{2.5}$  was observed at both BCN and MSY, and this relative increase was mostly due to SOA. Thus, based on our results, future increases of the SOA:POA ratio could cause an increase in  $E_{abs}$ .

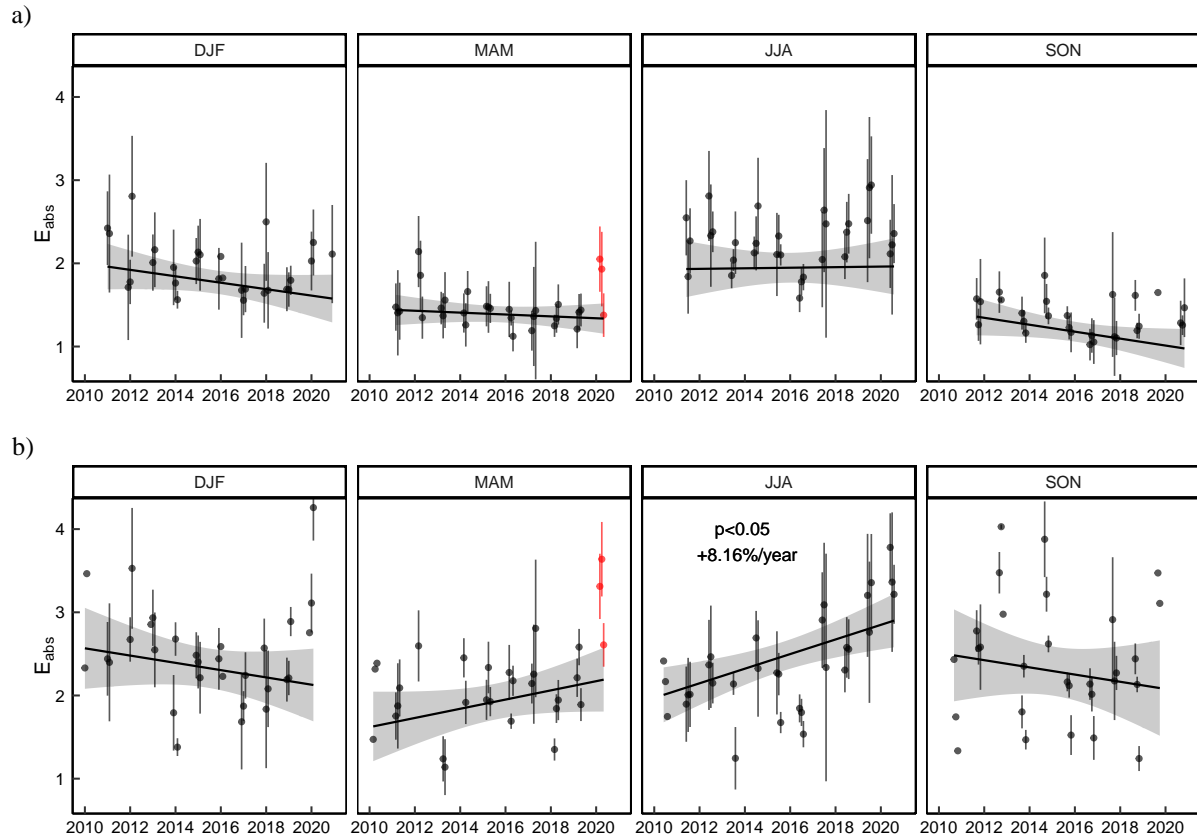


**Figure 6.** Absorption enhancement,  $E_{abs}$  at 637 nm seasonal trend analysis between 2011 and 2020 at a) Barcelona and b) Montseny station. The trend analysis was performed using a Theil-Sen function over the  $E_{abs}$  offline measurements.

#### 4 Conclusions

Here we have presented the results of the analysis of absorption enhancement analysis,  $E_{abs}$ , performed in Barcelona (BCN, 490 urban background) and Montseny (MSY, regional background) stations in the Mediterranean basin. We studied the main characteristics of  $E_{abs}$  and its dependence on other chemical compounds using both an intensive online measurement period in

BCN (2018), and a decade-long offline dataset (2010-2020) available at both BCN and MSY. The online approach consisted of co-located measurements at BCN of multi-wavelength absorption coefficients with an aethalometer (AE33), OC:EC analysis through a Semi-Continuous Sunset Analyzer, and non-refractory fine aerosol speciation and source apportionment with a Q-ACSM. The offline method consisted in comparing MAAP absorption coefficient measurements (at 637 nm) with offline 24-hour offline OC:EC measurements performed via a thermal-optical carbon analyser, SUNSET, following the EUSAAR2 protocol.

We calculated  $E_{abs}$  as the ratio between the ambient mass absorption cross-section (MAC) obtained from the measurements and the reference MAC value for pure BC particles. We have used two distinct reference MAC values: one based on an experimental site-specific MAC for pure BC, and a theoretical value from Bond and Bergstrom (2006). Using the site-specific reference MAC value, we reported  $E_{abs}$  values of  $1.28 \pm 0.36$ , and  $1.45 \pm 0.51$  for the online measurements at BCN at 880 nm and 370 nm, respectively, and of  $1.42 \pm 0.40$  and  $1.87 \pm 0.63$  for the offline analysis at BCN and MSY at 637 nm, respectively. The  $E_{abs}$  values reported in this work fall within the measured values reported in the literature (Liu et al., 2015; Zhang et al., 2018; Cappa et al., 2019). Moreover, our analysis confirmed the importance of OA particles as species that can increase  $E_{abs}$  when these are both internally and externally mixed with BC particles, as also reported in Zhang et al. (2018) for the Paris area (France)

We showed here that the seasonal behaviour of  $E_{abs}$  was a strong function of the wavelength used. In BCN we observed an increase of  $E_{abs}$  at the near-ultraviolet wavelengths during the cold period and we related the observed increase to the presence of brown carbon (BrC) particles externally mixed with BC particles. Conversely, in the red and near-infrared spectral range the  $E_{abs}$  variations were smaller. The relative contribution of BrC to the absorption enhancement increased from 4.6 % during the warm period up to 20.3% during the cold period, as expected due to the increase in the biomass burning activities during winter.  $E_{abs}$  at MSY at 637 nm showed an increase during the warm period, mainly associated to the larger contribution of secondary organic aerosols (SOA) affecting the regional station due to the larger emission of biogenic precursors in summer.

In this study we performed an analysis on the influence that the amount of material available for BC coating exerted on  $E_{abs}$ . We showed, in agreement with some prior studies, an exponential growth of  $E_{abs}$  with the amount of non-refractory aerosols. Thus, at the regional site, where the amount of material available for mixing reached higher values, so it did the  $E_{abs}$  values. Moreover, when evaluating between the different wavelengths for the online measurements, we obtained higher values for the short-UV wavelength (370 nm), in comparison with the near-infrared wavelengths (880 nm), which was associated with the presence of externally mixed BrC increasing the absorption at the shorter wavelengths.

The aging state influence on  $E_{abs}$  was examined using the triangular plot proposed by Ng et al. (2010) by means of the  $f_{44}$  and  $f_{43}$  factors derived from the Q-ACSM source analysis for online measurements at BCN station. We observed larger  $E_{abs}$  values for more aged organic aerosols, especially during the cold period, which was also related with a larger ratio of secondary-to-primary organic aerosols.

The long database of offline filter and MAAP measurements at both BCN and MSY allowed for a decade long seasonal trend analysis of  $E_{abs}$ . Overall, no statistically significant trends were observed at both stations. The exception, however, was the summer period at MSY regional station where a statistically significant increasing trend of 8.16 % per year was

observed for  $E_{abs}$ . This increase of  $E_{abs}$  at MSY in summer was mainly driven by a corresponding statistically significant increase of the OC:EC ratio. A previous study recently performed in the area under study, reported an increasing trend of the relative contribution of OA to PM and of SOA to OA with time at MSY regional station. Moreover, our analysis confirmed  
530 the importance of OA, and mostly of SOA, in contributing to the BC absorption enhancement. Furthermore, at both BCN and MSY the forced COVID-19 lockdown in spring 2020 implied a sharp increase of  $E_{abs}$ , mainly associated with the increase in the OC:EC ratio for this period due to the large reduction of anthropogenic emissions, and especially of BC particles, in the Barcelona urban environment. The observed statistically significant increasing trend of  $E_{abs}$  at MSY in summer, driven  
535 by a corresponding increase in the OC:EC ratio, suggested that  $E_{abs}$  could further increase during summer in the future due to the application of more restrictive measurements to reduce anthropogenic pollutant emissions. Thus, the higher absorption efficiency presented by the positive  $E_{abs}$  trend offsets, to some extent, the reduction of the absorption that would be associated to the decreasing trend of BC particles concentrations.

*Code and data availability.* The Montseny data sets used for this publication are accessible online on the WDCA (World Data Centre for  
540 Aerosols) web page: <http://ebas.nilu.no>. The Barcelona data sets were collected within different national and regional projects and/or agreements and are available upon request. The code used for analysis can be obtained upon request to the corresponding author.

*Author contributions.* AA, MCM, AK, NP, CR, MP, MV, and JYD carried out the maintenance and supervision of the instrumentation at BCN and MSY sites. AA, XQ, MCM, and MP helped in the processes of shaping the manuscript structure as well as with the data analysis. MV and MCM performed the analysis of the Q-ACSM data, and AK the measurements of OC and EC both online and offline. JYD processed and merged the different data-sets, analyzed the results, and summarized and expressed them in this manuscript. All authors provided advice  
545 regarding the structure and content as well as contributed to the writing of the final manuscript.

*Competing interests.* At the time of the research, MR and MI were also employed by the manufacturer of the Aethalometer AE33.

*Acknowledgements.* Measurements at Spanish sites (Barcelona, Montseny) were supported by the Spanish Ministry of Economy, Industry and Competitiveness and I+D+I "Retos Colaboración" funds under the CAIAC project (PID2019-108990PB-100), by FEDER funds (EQC2018-004598-P), by the Generalitat de Catalunya (AGAUR 2017 SGR41 and the DGQA) and the European Commission via ACTRIS-  
550 IMP (project 871115). We acknowledge support of the COST Action CA16109 COLOSSAL. IDAEA-CSIC is a Centre of Excellence Severo Ochoa (Spanish Ministry of Science and Innovation, Project CEX2018-000794-S). We would like to thank the Parc Natural i Reserva de la Biosfera del Montseny and the Diputació de Barcelona for the possibility of maintaining the regional background measurement station.

## References

Allan, J. D., Delia, A. E., Coe, H., Bower, K. N., Alfarra, M. R., Jimenez, J. L., Middlebrook, A. M., Drewnick, F., Onasch, T. B., Canagaratna, M. R., Jayne, J. T., and Worsnop, D. R.: A generalised method for the extraction of chemically resolved mass spectra from Aerodyne aerosol mass spectrometer data, *Journal of Aerosol Science*, 35, 909–922, <https://doi.org/10.1016/j.jaerosci.2004.02.007>, 2004.

555 Andreae, M. O. and Gelencsér, A.: Black carbon or brown carbon? the nature of light-absorbing carbonaceous aerosols, *Atmospheric Chemistry and Physics*, 6, 3131–3148, <https://doi.org/10.5194/acp-6-3131-2006>, 2006.

Bond, T. C. and Bergstrom, R. W.: Light absorption by carbonaceous particles: An investigative review, *Aerosol Science and Technology*, 560 40, 27–67, <https://doi.org/10.1080/02786820500421521>, 2006.

Bond, T. C., Doherty, S. J., Fahey, D., Forster, P., Berntsen, T., DeAngelo, B., Flanner, M., Ghan, S., Kärcher, B., Koch, D., et al.: Bounding the role of black carbon in the climate system: A scientific assessment, *Journal of Geophysical Research: Atmospheres*, 118, 5380–5552, 2013.

565 Brean, J., Beddows, D., Shi, Z., Temime-Roussel, B., Marchand, N., Querol, X., Alastuey, A., Minguillón, M. C., and Harrison, R. M.: Molecular insights into new particle formation in Barcelona, Spain, *Atmospheric Chemistry and Physics*, 20, 10 029–10 045, 2020.

Brines, M., Dall’Osto, M., Beddows, D. C., Harrison, R. M., and Querol, X.: Simplifying aerosol size distributions modes simultaneously detected at four monitoring sites during SAPUSS, *Atmospheric Chemistry and Physics*, 14, 2973–2986, <https://doi.org/10.5194/acp-14-2973-2014>, 2014.

570 Brines, M., Dall’Osto, M., Beddows, D. C., Harrison, R. M., Gómez-Moreno, F., Núñez, L., Artíñano, B., Costabile, F., Gobbi, G. P., Salimi, F., Morawska, L., Sioutas, C., and Querol, X.: Traffic and nucleation events as main sources of ultrafine particles in high-insolation developed world cities, *Atmospheric Chemistry and Physics*, 15, 5929–5945, <https://doi.org/10.5194/acp-15-5929-2015>, 2015.

Cappa, C. D., Onasch, T. B., Massoli, P., Worsnop, D. R., Bates, T. S., Cross, E. S., Davidovits, P., Hakala, J., Hayden, K. L., Jobson, B. T., Kolesar, K. R., Lack, D. A., Lerner, B. M., Li, S. M., Mellon, D., Nuaaman, I., Olfert, J. S., Petäjä, T., Quinn, P. K., Song, C., Subramanian, R., Williams, E. J., and Zaveri, R. A.: Radiative absorption enhancements due to the mixing state of atmospheric black carbon, *Science*, 337, 1078–1081, <https://doi.org/10.1126/science.1223447>, 2012.

575 Cappa, C. D., Zhang, X., Russell, L. M., Collier, S., Lee, A. K., Chen, C. L., Betha, R., Chen, S., Liu, J., Price, D. J., Sanchez, K. J., McMeeking, G. R., Williams, L. R., Onasch, T. B., Worsnop, D. R., Abbatt, J., and Zhang, Q.: Light Absorption by Ambient Black and Brown Carbon and its Dependence on Black Carbon Coating State for Two California, USA, Cities in Winter and Summer, *Journal of Geophysical Research: Atmospheres*, 124, 1550–1577, <https://doi.org/10.1029/2018JD029501>, 2019.

580 Cavalli, F., Viana, M., Yttri, K. E., Genberg, J., and Putaud, J.-P.: Toward a standardised thermal-optical protocol for measuring atmospheric organic and elemental carbon: the EUSAAR protocol, *Atmospheric Measurement Techniques*, 3, 79–89, 2010.

Chen, B., Bai, Z., Cui, X., Chen, J., Andersson, A., and Gustafsson, Ö.: Light absorption enhancement of black carbon from urban haze in Northern China winter, *Environmental Pollution*, 221, 418–426, <https://doi.org/10.1016/j.envpol.2016.12.004>, 2017.

585 Chen, Y., Xie, X., Shi, Z., Li, Y., Gai, X., Wang, J., Li, H., Wu, Y., Zhao, X., Chen, M., and Ge, X.: Brown carbon in atmospheric fine particles in Yangzhou, China: Light absorption properties and source apportionment, *Atmospheric Research*, 244, 105 028, <https://doi.org/10.1016/j.atmosres.2020.105028>, 2020.

City council of Barcelona, S. d. M.: Volum de trànsit (Intensitat mitjana diària de vehicles en dia feiner) a les principals vies. 2014-2018, 2014-2018, <https://www.bcn.cat/estadistica/catala/dades/anuaris/anuari19/cap15/C1511010.htm>, accessed: 2021-05-06.

590 Cui, X., Wang, X., Yang, L., Chen, B., Chen, J., Andersson, A., and Gustafsson, Ö.: Radiative absorption enhancement from coatings on black carbon aerosols, *Science of the Total Environment*, 551-552, 51–56, <https://doi.org/10.1016/j.scitotenv.2016.02.026>, 2016.

Dayan, U., Ricaud, P., Zbinden, R., and Dulac, F.: Atmospheric pollution over the eastern Mediterranean during summer—a review, *Atmospheric Chemistry and Physics*, 17, 13 233, 2017.

595 Drinovec, L., Močnik, G., Zotter, P., Prévôt, A., Ruckstuhl, C., Coz, E., Rupakheti, M., Sciare, J., Müller, T., Wiedensohler, A., and Hansen, A. D. A.: The "dual-spot" Aethalometer: an improved measurement of aerosol black carbon with real-time loading compensation, *Atmospheric Measurement Techniques*, 8, 1965–1979, 2015.

Ealo, M., Alastuey, A., Pérez, N., Ripoll, A., Querol, X., and Pandolfi, M.: Impact of aerosol particle sources on optical properties in urban, regional and remote areas in the north-western Mediterranean., *Atmospheric Chemistry & Physics*, 18, 2018.

European Commission, S.: 208 Final. Guidelines for Demonstration and Subtraction of Exceedances Attributable to Natural Sources Under the Directive 2008/50/EC on Ambient Air Quality and Cleaner Air for Europe, *Official Journal of the European Union*, 2011.

600 Evangelou, N., Platt, S. M., Eckhardt, S., Lund Myhre, C., Laj, P., Alados-Arboledas, L., Backman, J., Brem, B. T., Fiebig, M., Flentje, H., Marinoni, A., Pandolfi, M., Yus-Díez, J., Prats, N., Putaud, J. P., Sellegrí, K., Sorribas, M., Eleftheriadis, K., Vratolis, S., Wiedensohler, A., and Stohl, A.: Changes in black carbon emissions over Europe due to COVID-19 lockdowns, *Atmospheric Chemistry and Physics*, 21, 2675–2692, <https://doi.org/10.5194/acp-21-2675-2021>, 2021.

IPCC: Technical Summary. Contribution of Working Group I to the Sixth Assessment Report of the Intergovernmental Panel on Climate 605 Change, 2021.

Jacobson, M. Z.: Global direct radiative forcing due to multicomponent anthropogenic and natural aerosols, *Journal of Geophysical Research: Atmospheres*, 106, 1551–1568, 2001.

Karanasiou, A., Panteliadis, P., Perez, N., Minguillón, M. C., Pandolfi, M., Titos, G., Viana, M., Moreno, T., Querol, X., and Alastuey, A.: Evaluation of the Semi-Continuous OCEC analyzer performance with the EUSAAR2 protocol, *Science of the Total Environment*, 747, 610 <https://doi.org/10.1016/j.scitotenv.2020.141266>, 2020.

Kasthuriarachchi, N. Y., Rivellini, L. H., Adam, M. G., and Lee, A. K.: Light Absorbing Properties of Primary and Secondary Brown Carbon in a Tropical Urban Environment, *Environmental Science and Technology*, 54, 10 808–10 819, <https://doi.org/10.1021/acs.est.0c02414>, 2020.

Kirchstetter, T. W., Novakov, T., and Hobbs, P. V.: Evidence that the spectral dependence of light absorption by aerosols is affected by organic 615 carbon, *Journal of Geophysical Research D: Atmospheres*, 109, 1–12, <https://doi.org/10.1029/2004JD004999>, 2004.

Knox, A., Evans, G. J., Brook, J. R., Yao, X., Jeong, C. H., Godri, K. J., Sabaliauskas, K., and Slowik, J. G.: Mass absorption cross-section of ambient black carbon aerosol in relation to chemical age, *Aerosol Science and Technology*, 43, 522–532, <https://doi.org/10.1080/02786820902777207>, 2009.

Lack, D. A. and Cappa, C. D.: Impact of brown and clear carbon on light absorption enhancement, single scatter albedo and absorption 620 wavelength dependence of black carbon, *Atmospheric Chemistry and Physics*, 10, 4207–4220, <https://doi.org/10.5194/acp-10-4207-2010>, 2010.

Lack, D. A. and Langridge, J. M.: On the attribution of black and brown carbon light absorption using the Ångström exponent, *Atmospheric Chemistry and Physics*, 13, 10 535–10 543, <https://doi.org/10.5194/acp-13-10535-2013>, 2013.

Lack, D. A., Langridge, J. M., Bahreini, R., Cappa, C. D., Middlebrook, A. M., and Schwarz, J. P.: Brown carbon and internal mixing 625 in biomass burning particles, *Proceedings of the National Academy of Sciences of the United States of America*, 109, 14 802–14 807, <https://doi.org/10.1073/pnas.1206575109>, 2012.

Lack, D. A., Moosmüller, H., McMeeking, G. R., Chakrabarty, R. K., and Baumgardner, D.: Characterizing elemental, equivalent black, and refractory black carbon aerosol particles: A review of techniques, their limitations and uncertainties, *Analytical and Bioanalytical Chemistry*, 406, 99–122, <https://doi.org/10.1007/s00216-013-7402-3>, 2014.

630 Laskin, A., Laskin, J., and Nizkorodov, S. A.: Chemistry of Atmospheric Brown Carbon, *Chemical Reviews*, 115, 4335–4382, <https://doi.org/10.1021/cr5006167>, 2015.

Liu, S., Aiken, A. C., Gorkowski, K., Dubey, M. K., Cappa, C. D., Williams, L. R., Herndon, S. C., Massoli, P., Fortner, E. C., Chhabra, P. S., Brooks, W. A., Onasch, T. B., Jayne, J. T., Worsnop, D. R., China, S., Sharma, N., Mazzoleni, C., Xu, L., Ng, N. L., Liu, D., Allan, J. D., Lee, J. D., Fleming, Z. L., Mohr, C., Zotter, P., Szidat, S., and Prévôt, A. S.: Enhanced light absorption by mixed source black and brown carbon particles in UK winter, *Nature Communications*, 6, <https://doi.org/10.1038/ncomms9435>, 2015.

635 Minguillón, M. C., Ripoll, A., Pérez, N., Prévôt, A. S., Canonaco, F., Querol, X., and Alastuey, A.: Chemical characterization of submicron regional background aerosols in the western Mediterranean using an Aerosol Chemical Speciation Monitor, *Atmospheric Chemistry and Physics*, 15, 6379–6391, <https://doi.org/10.5194/acp-15-6379-2015>, 2015.

Moise, T., Flores, J. M., and Rudich, Y.: Optical Properties of Secondary Organic Aerosols and Their Changes by Chemical Processes, 640 *Chemical Reviews*, 115, 4400–4439, <https://doi.org/10.1021/cr5005259>, 2015.

Müller, T., Henzing, J., Leeuw, G. d., Wiedensohler, A., Alastuey, A., Angelov, H., Bizjak, M., Collaud Coen, M., Engström, J., Gruening, C., et al.: Characterization and intercomparison of aerosol absorption photometers: result of two intercomparison workshops, 2011.

645 Ng, N. L., Canagaratna, M. R., Zhang, Q., Jimenez, J. L., Tian, J., Ulbrich, I. M., Kroll, J. H., Docherty, K. S., Chhabra, P. S., Bahreini, R., Murphy, S. M., Seinfeld, J. H., Hildebrandt, L., Donahue, N. M., Decarlo, P. F., Lanz, V. A., Prévôt, A. S., Dinar, E., Rudich, Y., and Worsnop, D. R.: Organic aerosol components observed in Northern Hemispheric datasets from Aerosol Mass Spectrometry, *Atmospheric Chemistry and Physics*, 10, 4625–4641, <https://doi.org/10.5194/acp-10-4625-2010>, 2010.

Paatero, P.: The Multilinear Engine—A Table-Driven, Least Squares Program for Solving Multilinear Problems, Including the n-Way Parallel Factor Analysis Model, *Journal of Computational and Graphical Statistics*, 8, 854–888, <https://doi.org/10.1080/10618600.1999.10474853>, 1999.

650 Paatero, P. and Tapper, U.: Positive matrix factorization: A non-negative factor model with optimal utilization of error estimates of data values, *Environmetrics*, 5, 111–126, <https://doi.org/10.1002/env.3170050203>, 1994.

Pandolfi, M., Cusack, M., Alastuey, A., and Querol, X.: Variability of aerosol optical properties in the Western Mediterranean Basin, *Atmospheric Chemistry and Physics*, 11, 8189–8203, 2011.

655 Pandolfi, M., Querol, X., Alastuey, A., Jimenez, J., Jorba, O., Day, D., Ortega, A., Cubison, M., Comerón, A., Sicard, M., et al.: Effects of sources and meteorology on particulate matter in the Western Mediterranean Basin: An overview of the DAURE campaign, *Journal of Geophysical Research: Atmospheres*, 119, 4978–5010, 2014a.

Pandolfi, M., Ripoll, A., Querol, X., and Alastuey, A.: Climatology of aerosol optical properties and black carbon mass absorption cross section at a remote high-altitude site in the western Mediterranean Basin, *Atmospheric Chemistry and Physics*, 14, 6443–6460, 2014b.

660 Pandolfi, M., Alastuey, A., Pérez, N., Reche, C., Castro, I., Shatalov, V., and Querol, X.: Trends analysis of PM source contributions and chemical tracers in NE Spain during 2004–2014: a multi-exponential approach, *Atmospheric Chemistry and Physics*, 16, 11 787–11 805, 2016.

Peng, J., Hu, M., Guo, S., Du, Z., Zheng, J., Shang, D., Zamora, M. L., Zeng, L., Shao, M., Wu, Y. S., Zheng, J., Wang, Y., Glen, C. R., Collins, D. R., Molina, M. J., and Zhang, R.: Markedly enhanced absorption and direct radiative forcing of black carbon un-

der polluted urban environments, *Proceedings of the National Academy of Sciences of the United States of America*, 113, 4266–4271, 665 <https://doi.org/10.1073/pnas.1602310113>, 2016.

Pérez, N., Pey, J., Castillo, S., Viana, M., Alastuey, A., and Querol, X.: Interpretation of the variability of levels of regional background aerosols in the Western Mediterranean, *Science of the total environment*, 407, 527–540, 2008.

Petzold, A. and Schönlinner, M.: Multi-angle absorption photometry—a new method for the measurement of aerosol light absorption and atmospheric black carbon, *Journal of Aerosol Science*, 35, 421–441, 2004.

670 Pey, J., Pérez, N., Castillo, S., Viana, M., Moreno, T., Pandolfi, M., López-Sébastián, J., Alastuey, A., and Querol, X.: Geochemistry of regional background aerosols in the Western Mediterranean, *Atmospheric Research*, 94, 422–435, 2009.

Qin, Y. M., Bo Tan, H., Li, Y. J., Jie Li, Z., Schurman, M. I., Liu, L., Wu, C., and Chan, C. K.: Chemical characteristics of brown carbon in atmospheric particles at a suburban site near Guangzhou, China, *Atmospheric Chemistry and Physics*, 18, 16 409–16 418, 675 <https://doi.org/10.5194/acp-18-16409-2018>, 2018.

Querol, X., Alastuey, A., Rodriguez, S., Plana, F., Ruiz, C. R., Cots, N., Massagué, G., and Puig, O.: PM10 and PM2.5 source apportionment in the Barcelona Metropolitan area, Catalonia, Spain, *Atmospheric Environment*, 35, 6407–6419, 2001.

Querol, X., Pey, J., Pandolfi, M., Alastuey, A., Cusack, M., Pérez, N., Moreno, T., Viana, M., Mihalopoulos, N., Kallos, G., et al.: African dust contributions to mean ambient PM10 mass-levels across the Mediterranean Basin, *Atmospheric Environment*, 43, 4266–4277, 2009.

Querol, X., Massagué, J., Alastuey, A., Moreno, T., Gangoiti, G., Mantilla, E., Duéguez, J. J., Escudero, M., Monfort, E., García-Pando, 680 C. P., et al.: Lessons from the COVID-19 air pollution decrease in Spain: Now what?, *Science of The Total Environment*, 779, 146 380, 2021.

Reche, C., Querol, X., Alastuey, A., Viana, M., Pey, J., Moreno, T., Rodríguez, S., González, Y., Fernández-Camacho, R., Rosa, J., et al.: New considerations for PM, Black Carbon and particle number concentration for air quality monitoring across different European cities, *Atmospheric Chemistry and Physics*, 11, 6207–6227, 2011.

685 Rigler, M., Drinovec, L., Lavri, G., Vlachou, A., Prevot, A. S., Luc Jaffrezo, J., Stavroulas, I., Sciare, J., Burger, J., Kranjc, I., Turšič, J., D. A. Hansen, A., and Mocnik, G.: The new instrument using a TC-BC (total carbon-black carbon) method for the online measurement of carbonaceous aerosols, *Atmospheric Measurement Techniques*, 13, 4333–4351, <https://doi.org/10.5194/amt-13-4333-2020>, 2020.

Rivas, I., Beddows, D. C., Amato, F., Green, D. C., Järvi, L., Hueglin, C., Reche, C., Timonen, H., Fuller, G. W., Niemi, J. V., et al.: Source apportionment of particle number size distribution in urban background and traffic stations in four European cities, *Environment 690 International*, 135, 105 345, 2020.

Rodríguez, S., Querol, X., Alastuey, A., Kallos, G., and Kakaliagou, O.: Saharan dust contributions to PM10 and TSP levels in Southern and Eastern Spain, *Atmospheric Environment*, 35, 2433–2447, 2001.

Rodríguez, S., Querol, X., Alastuey, A., and Plana, F.: Sources and processes affecting levels and composition of atmospheric aerosol in the western Mediterranean, *Journal of Geophysical Research: Atmospheres*, 107, AAC–12, 2002.

695 Saleh, R.: From Measurements to Models: Toward Accurate Representation of Brown Carbon in Climate Calculations, *Current Pollution Reports*, 6, 90–104, <https://doi.org/10.1007/s40726-020-00139-3>, 2020.

Saleh, R., Cheng, Z., and Atwi, K.: The Brown-Black Continuum of Light-Absorbing Combustion Aerosols, *Environmental Science and Technology Letters*, 5, 508–513, <https://doi.org/10.1021/acs.estlett.8b00305>, 2018.

Samset, B. H., Sand, M., Smith, C. J., Bauer, S. E., Forster, P. M., Fuglestvedt, J. S., Osprey, S., and Schleussner, C. F.: Climate Impacts From 700 a Removal of Anthropogenic Aerosol Emissions, *Geophysical Research Letters*, 45, 1020–1029, <https://doi.org/10.1002/2017GL076079>, 2018.

Seco, R., Peñuelas, J., Filella, I., Llusia, J., Schallhart, S., Metzger, A., Müller, M., and Hansel, A.: Volatile organic compounds in the western Mediterranean basin: Urban and rural winter measurements during the DAURE campaign, *Atmospheric Chemistry and Physics*, 13, 4291–4306, <https://doi.org/10.5194/acp-13-4291-2013>, 2013.

705 Tobías, A., Carnerero, C., Reche, C., Massagué, J., Via, M., Minguillón, M. C., Alastuey, A., and Querol, X.: Changes in air quality during the lockdown in Barcelona (Spain) one month into the SARS-CoV-2 epidemic, *Science of the total environment*, 726, 138 540, 2020.

Veld, M. i. t., Alastuey, A., Pandolfi, M., Amato, F., Pérez, N., Reche, C., Via, M., Minguillón, M. C., Escudero, M., and Querol, X.: Compositional changes of PM<sub>2.5</sub> in NE Spain during 2009–2018: A trend analysis of the chemical composition and source apportionment, *Science of the Total Environment*, 795, <https://doi.org/10.1016/j.scitotenv.2021.148728>, 2021.

710 Via, M., Minguillón, M. C., Reche, C., Querol, X., and Alastuey, A.: Increase in secondary organic aerosol in an urban environment, *Atmospheric Chemistry and Physics*, 21, 8323–8339, <https://doi.org/10.5194/acp-21-8323-2021>, 2021.

Viana, M., Chi, X., Maenhaut, W., Cafmeyer, J., Querol, X., Alastuey, A., Mikuška, P., and Večeřa, Z.: Influence of sampling artefacts on measured PM, OC, and EC levels in carbonaceous aerosols in an urban area, *Aerosol Science and Technology*, 40, 107–117, <https://doi.org/10.1080/02786820500484388>, 2006.

715 Wu, Y., Cheng, T., Liu, D., Allan, J. D., Zheng, L., and Chen, H.: Light Absorption Enhancement of Black Carbon Aerosol Constrained by Particle Morphology, *Environmental Science and Technology*, 52, 6912–6919, <https://doi.org/10.1021/acs.est.8b00636>, 2018.

Xu, X., Zhao, W., Qian, X., Wang, S., Fang, B., Zhang, Q., Zhang, W., Venables, D. S., Chen, W., Huang, Y., Deng, X., Wu, B., Lin, X., Zhao, S., and Tong, Y.: The influence of photochemical aging on light absorption of atmospheric black carbon and aerosol single-scattering albedo, *Atmospheric Chemistry and Physics*, 18, 16 829–16 844, <https://doi.org/10.5194/acp-18-16829-2018>, 2018.

720 Yus-Díez, J., Ealo, M., Pandolfi, M., Perez, N., Titos, G., Močnik, G., Querol, X., and Alastuey, A.: Aircraft vertical profiles during summertime regional and Saharan dust scenarios over the north-western Mediterranean Basin: aerosol optical and physical properties, *Atmospheric Chemistry and Physics Discussions*, pp. 1–35, 2020.

Yus-Díez, J., Bernardoni, V., Močnik, G., Alastuey, A., Ciniglia, D., Ivančić, M., Querol, X., Perez, N., Reche, C., Rigler, M., Vecchi, R., Valentini, S., and Pandolfi, M.: Determination of the multiple-scattering correction factor and its cross-sensitivity to scattering and wavelength dependence for different AE33 Aethalometer filter tapes: A multi-instrumental approach, *Atmospheric Measurement Techniques Discussions*, 29, 1–30, <https://doi.org/10.5194/amt-2021-46>, 2021.

725 Zanatta, M., Gysel, M., Bukowiecki, N., Müller, T., Weingartner, E., Areskoug, H., Fiebig, M., Yttri, K. E., Mihalopoulos, N., Kouvarakis, G., et al.: A European aerosol phenomenology-5: Climatology of black carbon optical properties at 9 regional background sites across Europe, *Atmospheric environment*, 145, 346–364, 2016.

730 Zhang, Y., Favez, O., Canonaco, F., Liu, D., Močnik, G., Amodeo, T., Sciare, J., Prévôt, A. S. H., Gros, V., and Albinet, A.: Evidence of major secondary organic aerosol contribution to lensing effect black carbon absorption enhancement, *npj Climate and Atmospheric Science*, 1, <https://doi.org/10.1038/s41612-018-0056-2>, 2018.

Zhang, Y., Albinet, A., Petit, J. E., Jacob, V., Chevrier, F., Gille, G., Pontet, S., Chrétien, E., Dominik-Sègue, M., Levigoureux, G., Močnik, G., Gros, V., Jaffrezo, J. L., and Favez, O.: Substantial brown carbon emissions from wintertime residential wood burning over France, *Science of the Total Environment*, 743, <https://doi.org/10.1016/j.scitotenv.2020.140752>, 2020.